Final Report for
DUSEL R&D: BetaCage:
A Screener of Ultra-Low-Level Radioactive Surface Contamination
DE-FG02-07ER41481
PI: S. Golwala (Caltech)
$172,000
7/15/2007–7/14/2011

1 Introduction

Underground physics experiments include studies of solar neutrinos, searches for neutrinoless $\beta\beta$ decay, and efforts to detect a new subatomic particle candidate for the dark matter pervading the Universe. These experiments must be built from low-radioactivity components. Existing screening facilities are insufficiently sensitive to meet all the needs of planned experiments, in particular testing for low-energy electron emitters and alpha-decaying isotopes [1, 2, 3, 4, 5]. With this grant, we developed a prototype of such a detector, the BetaCage [6, 7, 8, 9]. The eventual full-size, radiopure BetaCage will be a low-background, atmospheric-pressure neon drift chamber with unprecedented sensitivity to emitters of low-energy electrons and alpha particles. We expect that the prototype BetaCage already developed will be an excellent screener of alpha particles. Both the prototype and final BetaCage will provide new infrastructure for rare-event science as well as for a wider community that makes use of radioactive screening for areas such as archeology, biology, climatology, environmental science, geology, integrated-circuit quality control, and planetary science.

2 The Need for the BetaCage

Traditionally, experimenters have used high-purity germanium ionization (HPGe) detectors to obtain high-resolution spectra of gamma-ray emission from tens of keV to a few MeV, which enables the identification of contaminants by their characteristic gamma rays. However, HPGe screening may be insufficient for screening contaminants that beta decay without associated high-energy gamma-ray emission. Mass spectroscopy is sensitive enough to search for some of these isotopes. Nevertheless, of the 79 isotopes listed in Table 1 that decay by beta emission or electron capture[1], as many as 26 are inaccessible unless α or β screening is employed, or one is able to obtain an extraordinary 1 ppt sensitivity with mass spectrometry. Mass spectroscopy also is destructive and usually requires sample processing that may introduce new contaminants or cloud the relation between the intrinsic contamination level and the measured signal.

A particularly dangerous contamination for a number of underground physics experiments is the deposition of radon daughters from the atmosphere, which decay to the long-lived ^{210}Pb, a low-energy beta emitter, and then to the alpha-emitting ^{210}Po, with no penetrating radioactivity signature. The beta emitter has been the dominant background for the dark matter experiments SuperCDMS [10], EDELWEISS [11], and XMASS [12, 13]. The alpha emitter has dominated the double-beta decay experiment, CUORE [14, 15], and is critical for the large number of dark

---

[1] Isotopes that decay via electron capture have associated low-energy X-rays and/or Auger electrons, which are emitted in the process of filling the vacancy created by the electron capture.

Method	Long-lived Beta-Emitting or Electron-Capture Isotopes
ICP-MS (1 ppb)	^{40}K ^{48}Ca ^{50}V ^{87}Rb ^{92}Nb ^{98}Tc ^{113}Cd ^{115}In ^{123}Te ^{138}La ^{176}Lu ^{182}Hf ^{232}Th ^{235}U ^{238}U ^{236}Np ^{250}Cm
ICP-MS (1 ppt)	^{10}Be ^{36}Cl ^{60}Fe ^{79}Se ^{93}Zr ^{94}Nb ^{97}Tc ^{99}Tc ^{107}Pd ^{126}Sn ^{129}I ^{135}Cs ^{137}La ^{154}Eu ^{158}Tb ^{166m}Ho ^{208}Bi ^{208}Po ^{209}Po ^{252}Es
γ	^{40}K ^{50}V ^{60}Fe ^{60}Co ^{93}Zr ^{92}Nb ^{94}Nb ^{93}Mo ^{98}Tc ^{99}Tc ^{101}Rh ^{101m}Rh ^{102m}Rh ^{109}Cd ^{121m}Sn ^{126}Sn ^{125}Sb ^{129}I ^{134}Cs ^{137}Cs ^{133}Ba ^{138}La ^{145}Pm ^{146}Pm ^{150}Eu ^{152}Eu ^{154}Eu ^{155}Eu ^{157}Tb ^{158}Tb ^{166m}Ho ^{173}Lu ^{174}Lu ^{176}Lu ^{172}Hf ^{179}Ta ^{207}Bi ^{208}Bi ^{232}Th ^{235}U ^{238}U ^{236}Np ^{241}Pu
α	^{210}Pb ^{208}Po ^{209}Po ^{228}Ra ^{227}Ac ^{232}Th ^{235}U ^{238}U ^{236}Np ^{241}Pu ^{250}Cm ^{252}Es
β/ppt MS	^{10}Be ^{36}Cl ^{79}Se ^{97}Tc ^{107}Pd ^{135}Cs ^{137}La ^{154}Eu ^{209}Po
β only	^{3}H ^{14}C ^{32}Si ^{63}Ni ^{90}Sr ^{106}Ru ^{113m}Cd ^{147}Pm ^{151}Sm ^{171}Tm ^{194}Os ^{204}Tl

Table 1: Detection schemes for all long-lived beta-emitting or electron-capture isotopes. ICP-MS (inductively-coupled-plasma mass spectroscopy) is listed both with its commonly achieved sensitivity of 1 ppb and with a better sensitivity of 1 ppt, which has been achieved for some isotopes. Many isotopes (including ^{210}Pb) can be screened effectively only by emission of their beta electrons or alphas, and some can be detected only by their beta emission or by ICP-MS with sensitivity between 1 ppb and 1 ppt.

matter and neutrino experiments that use liquids within containment vessels. Experiments such as CLEAN [16] and DEAP [17] define fiducial regions well away from the container walls in order to reject the short-range alphas, but a sufficiently high rate of alphas will render nonnegligible the probability of misreconstructing such events into the fiducial region. For COUPP [18, 19], movement of the parent nucleus from the surface into the bulk may produce a background, and too high a surface alpha event rate would cause significant dead time. Finally, for many experiments (*e.g.* XENON1T [20], LZ [21], and DArKSIDE [22]) (α, n) reactions from surface contamination may be a significant background.

In this case, the ^{210}Po alpha emitter is out of equilibrium with the photon-emitting isotopes in its parent ^{238}U decay chain because the uranium parent has been chemically separated. Direct detection of the alpha (or a beta from the nearby parent ^{210}Pb or ^{210}Bi) is necessary to establish the alpha-emitter contamination level. Screening based on detecting the betas from ^{210}Pb or ^{210}Bi has a significantly better sensitivity than the alpha screening if the contamination is due to recent exposure to radon (or to ^{210}Pb) since it takes significant time for the ^{210}Po daughter to "grow in."

The common challenge of detecting low-energy betas and alphas is that the particles cannot penetrate through a vacuum window or through the dead layer of a conventional HPGe detector. Even special-purpose detectors with very thin dead layers (e.g., Si(Li), B-implanted HPGe, or silicon surface-barrier detectors) have deficiencies: there remains a vacuum window that may stop or scatter some particles, backscattering effects distort the energy spectrum, and it is difficult to obtain the $\sim$m^2 sensitive area desired for high screening throughput and to minimize edge effects.

3 Detector Design

3.1 Overview

An ideal detector would place the sample directly in the detection medium (*e.g.* a gas) to eliminate backscattering and dead layer effects while providing a large sensitive area. The BetaCage, an ultra-low-background drift chamber, is designed around this principle to optimize detection of $\lesssim$ 200 keV electrons and alpha particles from a sample's surface. Three goals guided the design from this starting point. First, the detector should use the minimum amount of gas needed to stop particles of interest in order to minimize background from ambient penetrating gammas. Second, the detector should have the minimum possible surface area that itself can be a source

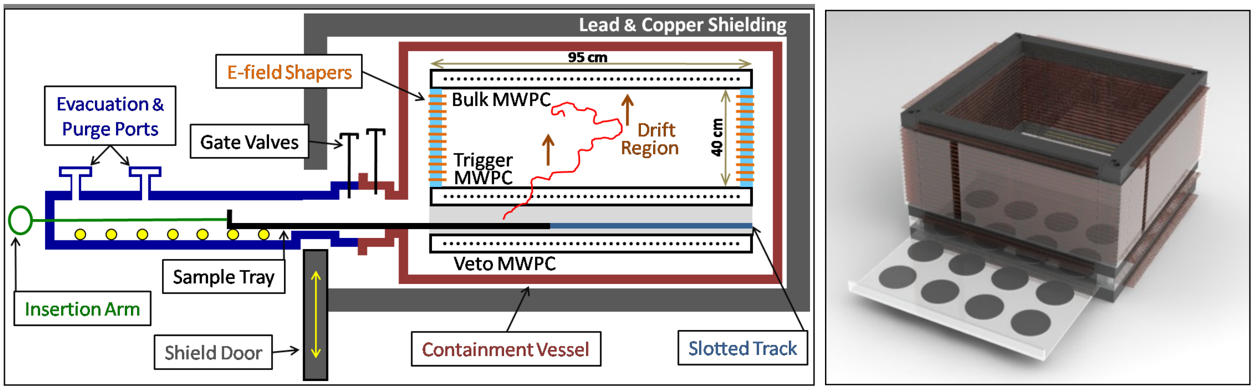

Figure 1: Left: Schematic side view of the BetaCage. The trigger, bulk, and veto MWPCs are indicated, as is the location of the sample. The outer region indicates the gamma shielding. Right: CAD drawing of BetaCage MWPCs and field-shaping structure, with sample tray partially removed. No shield or load-lock is shown here.

of background particles. Third, the detector should provide sufficient spatial information about events to distinguish between those coming from the sample surface and those due to scattering of background particles in the gas.

Figure 1 shows a sketch and CAD drawing of the full-size BetaCage. Samples are placed in the gas. An open multi-wire proportional counter (MWPC) directly above the sample provides a trigger for particles emanating from the sample. Above this "trigger" MWPC is a large region in which the emitted particles stop. The depth and width of the drift region sets the energy of betas whose full energy is contained in the detector. An electric field in this region drifts the ionization to the top of the chamber, where a second open ("bulk") MWPC collects it. Proportional avalanching in both MWPCs provides gain. Crossed grids in both MWPCs provide x–y position determination. The time profile of charge collection in the bulk MWPC determines the spatial profile of the track in the z dimension. The trigger MWPC provides a start time to establish absolute z location.

We chose neon gas at STP based on desired stopping power, feasibility of purification, drift properties (drift speed, diffusion, electron attachment length), and avalanche gain. Neon's stopping power is large enough that a 30-cm-high drift region will contain greater than 90% of 150-keV betas, so the full spectrum of electrons from likely low-energy emitters such as ^{14}C, ^{210}Pb, etc., will be contained in the chamber. Likewise, even a 10-MeV alpha particle will be contained in a 20-cm-high drift region. Yet the stopping power is low enough that the trigger MWPC can be thick enough (1 cm) to make assembly straightforward, and the gamma background is sufficiently low in a shield of moderate cost and size. Neon has no long-lived naturally occurring unstable isotopes, so purification by chemical means is sufficient (in contrast to argon).

The design minimizes backgrounds due to the chamber itself and provides excellent rejection of residual and unavoidable backgrounds. By design, the only surface of the detector near the sample is that of the wires, whose area is only a few percent of the sample surface area. Events whose tracks do not have one end at the sample and the other inside the drift region will be vetoed using the full 3D information. A third, "veto" MWPC below the sample vetoes throughgoing events.

As shown in Table 2, with appropriate construction materials, the limiting background in the BetaCage is ejection of electrons from the sample surface by Compton-scattering photons from contamination external to the detector itself [6]. A radon-purged 15-cm lead shield surrounding 5 cm of lead with $< 10\,\mathrm{Bq/kg}$ ^{210}Pb and a 1-cm copper liner in the Soudan Underground Laboratory's DOE-funded Low-Background Counting Facility (LBCF) should yield external photon rates that would result in $\sim 1\,\mathrm{keV}^{-1}\mathrm{kg}^{-1}\mathrm{day}^{-1}$ in a HPGe detector, based on past efforts [23, 24] and

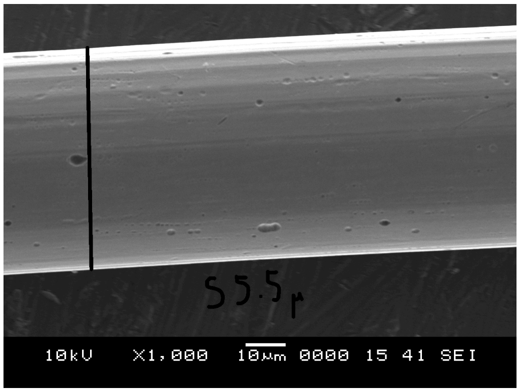

Figure 2: Image of an originally 65-micron-diameter stainless steel wire after 2 minutes of electropolishing, which reduced the diameter about 9 microns.

Source	Rate ($\mathrm{keV^{-1}\,m^{-2}\,day^{-1}}$)
Gammas, equivalent to $1\,\mathrm{keV^{-1}kg^{-1}day^{-1}}$in Ge	3×10^{-1}
5% methane quench gas (assumed with $^{14}\mathrm{C}/^{12}\mathrm{C} = 10^{-16}$)	5×10^{-2}
Wires: emergent beta rate $< 100\,\mathrm{keV}$	$\approx 10^{-4}$
Wires: rate from gammas in full volume	$\approx 10^{-9}$
30 resistors: Rate from gammas in full volume	$\approx 10^{-2}$
Noryl frames: Rate from gammas in full volume	3×10^{-1}
copper field shapers: Rate from gammas in full volume	$\approx 10^{-4}$
acrylic spacers and vessel: Rate from gammas in full volume	$\approx 10^{-1}$
stainless steel feedthrough tube and gate valve: Rate from gammas in full volume	$\approx 10^{-3}$

Table 2: Expected contributions to beta background levels in the BetaCage. The first line "Gammas" refers to gammas from the surrounding shielding material, consisting of the lead shield and copper liner. More detailed background estimates are given in Figure 13.

simulations [25]. The LBCF has a 280-square-foot class-10,000 clean room that will provide us with the needed 5' × 8' experimental space at a depth of 2030 meters of water equivalent, with signals from an active veto shield enclosing the entire 35-m × 40-m × 100-m cavern.

To minimize gamma emission from the detector itself, the chamber and enclosing vessel will be constructed from plastics and copper, with a small amount of stainless steel. A dogleg in the stainless steel tube carrying cabling to feedthrough ports outside the shielding will minimize contributions from feedthroughs and front-end electronics. Our gas-handling system will pass the neon through cooled charcoal to remove radon and krypton (see *e.g.* [26, 27]). Radon daughter plate-out onto the wires will be removed by electropolishing [28, 29], as we have demonstrated in Figure 2, prior to stringing the wires in an ultra-low-radon cleanroom [30]. Other background sources, including $^{14}\mathrm{C}$ in the methane quench gas (assuming a conservative ratio of $^{14}\mathrm{C}/^{12}\mathrm{C}$ of 10^{-16} [31, 32]), uranium and thorium in the stainless steel, and resistors for the drift-field shaper voltage divider, will be subdominant.

The expected ambient photon background of $1\,\mathrm{keV^{-1}kg^{-1}day^{-1}}$ will yield a Compton-scatter rate of 0.3 $\mathrm{keV^{-1}\,m^{-2}\,day^{-1}}$ ejected electrons. To reach the 0.1 $\mathrm{keV^{-1}\,m^{-2}\,day^{-1}}$ target sensitivity thus requires background subtraction. One day of background measurement would establish a 60 $\mathrm{m^{-2}}$ $\mathrm{day^{-1}}$ background rate over 0 to 200 keV to a precision of $7.7\,\mathrm{m^{-2}}$ $\mathrm{day^{-1}}$, allowing detection at almost 3σ of a 0.1 $\mathrm{keV^{-1}\,m^{-2}\,day^{-1}}$ rate contaminant in a total of 2 days of running (excluding sample installation and purging of the chamber). Fifteen days counting each for sample and background would allow a sensitivity of 0.04 $\mathrm{keV}^{-1}\,\mathrm{m}^{-2}\,\mathrm{day}^{-1}$ rate. Even for a background rate 10× higher than expected, fifteen days counting each for sample and background would yield a sensitivity of 0.13 $\mathrm{keV}^{-1}\,\mathrm{m}^{-2}\,\mathrm{day}^{-1}$ rate.

The BetaCage (both the full-size version and the prototype) will be an excellent alpha screener thanks to the uniquely short, dense, straight, high-energy tracks resulting from alpha interactions. Gamma rays from natural radioactivity are not high enough in energy to be mistaken for surface alphas. In its underground, shielded environment, unvetoed backgrounds from cosmic rays should be negligible. The dominant background to alpha counting is expected to be from radon daughters in the gas itself that happen to decay in a position and direction that allows their track to mimic one from the sample or that plate out onto the sample itself. These will be mitigated by the cold trap and circulation of the gas.

The most sensitive commercial alpha detector, the XIA UltraLo-1800 [36], also a gas chamber (using Ar), has demonstrated backgrounds as low as 20 $\mathrm{m}^{-2}\,\mathrm{day}^{-1}$ with a 0.18 m^2 sample area. With the BetaCage's design advantages (cleaner gas, lower surface area of material in the fiducial region, tracking, shielded operation underground, etc.), we expect an alpha background $\gtrsim 100\times$ lower. For two weeks counting, the expected sensitivity $\sim 0.1\,\mathrm{counts}\,\mathrm{m}^{-2}\,\mathrm{day}^{-1}$.

The energy resolution of the BetaCage will be worse than that of Si(Li) or B-implanted HPGe detectors, or conventional Si barrier detector technology. However, as shown in Section 4, the resolution should be sufficient to allow identification of beta emission spectra by their endpoint energy (or to identify alphas). The advantage of better sensitivity is more important.

3.2 MWPC and Drift Region Electrostatic Design

Each MWPC in the BetaCage consists of 3 planes of wires: a central anode plane and two cathode planes. The electrostatic design of the MWPC unit cell is illustrated in Figure 3.

The voltages on the MWPC grids set the gain via the Diethorn formula

$$\ln G = \frac{\ln 2}{\Delta V}\frac{\lambda}{2\pi\epsilon_0}\ln\frac{\lambda}{2\pi\epsilon_0\, r_0\, E_{\mathrm{min}}(\rho_0)\,\rho/\rho_0} \tag{1}$$

where G is the gain, $\Delta V \approx 41$ V (90%/10% Ne/CH_4) is the potential difference through which an electron must be accelerated to ionize a gas molecule, λ is line charge density for a given voltage, r_0 is the wire radius, $E_{\mathrm{min}} \approx 10$ kV/cm (90%/10% Ne/CH_4) is the electric field needed to start an avalanche, ρ is the gas density, ρ_0 is the gas density at STP, and ϵ_0 is the permittivity of free space (see, e.g., [37]). ΔV and E_{min} are calculated using GARFIELD[2]. Gains of approximately 10^4 for the bulk MWPC and 10^5 for the trigger MWPC are sufficient to overcome electronics noise. Fortunately, the exponential dependence of gain on voltage (via λ) makes both gains achievable with modest voltage differences of roughly 1100 to 1300 V, as shown in Fig. 3. Because our calculations do not take into account the Penning effect, the gains obtained in practice will be larger. Gain is easily calibrated *in situ* using 6 keV X-rays, as shown in Figure 8.

The desired gains are achieved with wire spacing of 5 mm (in-plane and between planes), which yields a reasonable total wire count for the structure (151 per wire plane) while also providing fine enough position resolution that track diffusion rather than wire spacing is limiting. The anode wires are 25 μm and the cathode wires 125 μm in diameter.

In the prototype BetaCage, we have a drift volume of 41 cm by 41 cm by 22 cm, while the full-size BetaCage will have a drift volume of 80 cm by 80 cm by 40 cm. The prototype BetaCage is designed for 200 keV electrons to range out in P10 (90%/10% Ar/CH_4) while the full-size BetaCage is designed for 90%/10% or 95%/5% Ne/CH_4 . We will use a Ne/CH_4 mixture for the

---

[2] `http://garfield.web.cern.ch/garfield/`

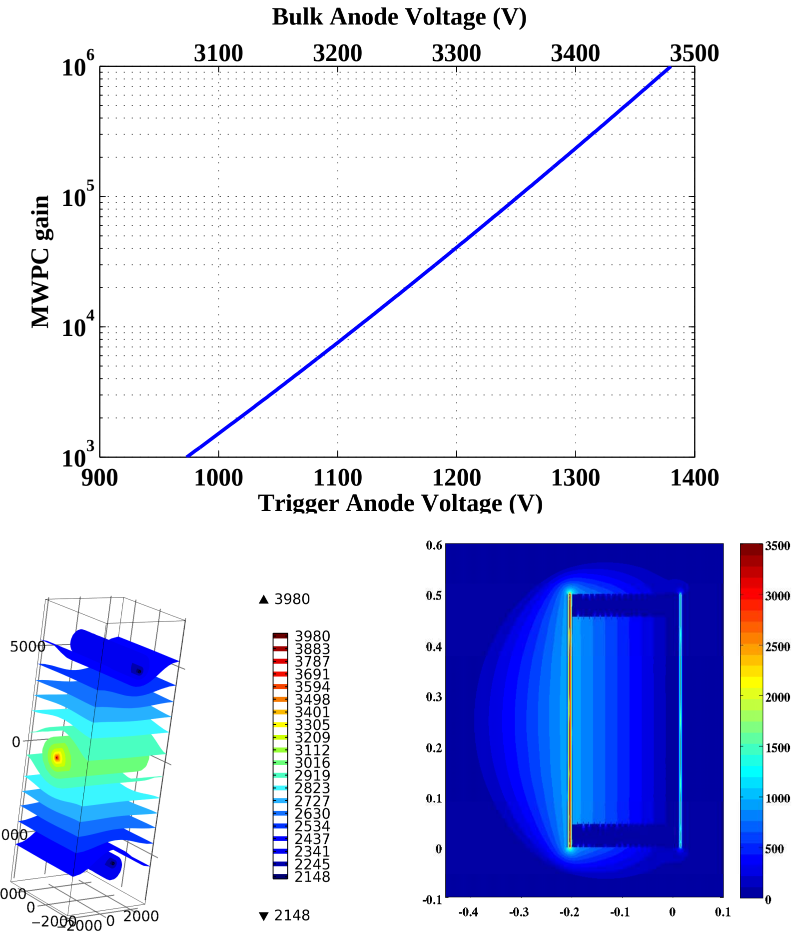

Figure 3: BetaCage electrostatic design. Top: MWPC gain as a function of trigger MWPC anode voltage (cathode set to 0 V) and bulk MWPC anode voltage (cathode set to 2100 V). Bottom left: Equipotential surfaces for a single MWPC cell. The anode wire runs down the center and the cathode wires are at top and bottom. The scales along the axes indicate distance in μm. The voltages are indicated at right. Bottom right: Potential map of the entire structure. The two high-field regions are the MWPCs, the trigger at right and the bulk at left. The uniform electric field in the drift region in the center is visible, set by the field shapers placed between the two MWPCs. The behavior of the field outside the field shapers and MWPCs is determined by the surrounding grounded metal vacuum vessel.

BetaCage instead of well-characterized Ar/CH_4 because argon has a long-lived naturally occurring radioactive isotope, ^{39}Ar. Because contamination by ^{14}C in the quench gas is a consideration, we will experiment with use of a CH_4 fraction of 5%. The drift field is determined by requiring that ionization track diffusion over the drift distance is small compared to the 5-mm wire spacing (so the wire density is not excessive). The expected drift velocities are 3.5 cm/μs for P10 and 1.7 cm/μs (1.6 cm/μs) for 90%/10% (95%/5%) Ne/CH_4, while the corresponding diffusion at 50 V/cm is expected to be 628 $\mu\text{m}/\sqrt{\text{cm}}$ for P10 and 471 $\mu\text{m}/\sqrt{\text{cm}}$ (498 $\mu\text{m}/\sqrt{\text{cm}}$) for Ne/$CH_4$. For both the 20-cm drift region in the prototype with P10 and the 40-cm-drift region in the full-size version with Ne/CH_4, we expect 3–4 mm of diffusion. To achieve 50 V/cm, the trigger MWPC cathode is held at 0 V and the bulk MWPC cathode at 2100 V. The large-scale electrostatic field configuration is shown in Figure 3.

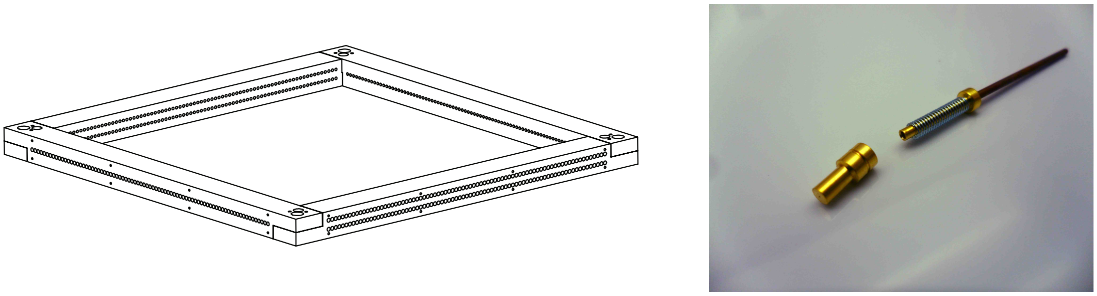

Figure 4: Left: MWPC frame, composed of Noryl, showing the holes for the wire feedthroughs. Right: Spring-loaded wire feedthrough. A wire passes through the hole in the center of the left brass part, through the right brass part and into the copper tube, where it is crimped.

3.3 MWPC and Drift Region Mechanical Design

The driving concerns for the MWPC design are gain stability, gain uniformity, and radiopurity. It is the most challenging aspect of the detector.

Gain stability and uniformity is required so that the energy resolution of the design, set by ionization creation statistics and readout noise, is not degraded by variation of gain with position across the MWPC or with time. Considering fluctuations in Equation 1, we find that 5% variation in gain arises from 2.5 V ($\sim 0.2\%$) variation in voltage, 1.5% variation in anode wire diameter, or 100 μm (2%) variation in wire spacing. While voltage stability is easily achieved with commercial units, the constraints on machining, assembly precision, and stability are stringent. Tensioned wires are necessary, where 20-g and 200-g tensions for the anode and cathode wires, respectively, limit sag under gravitational and electrostatic forces to less than 30 μm, yielding $< 1\%$ gain variations.

The radiopurity challenge leads us away from standard MWPC construction materials like G-10 and metals in favor of plastics. Noryl is acceptable: screening with the UMN Gopher HPGe detector and the UC Davis neutron-activation technique demonstrates contamination levels no worse than 5 mBq/kg ^{238}U, ^{232}Th, and ^{40}K, quite acceptable, yet Noryl is also strong enough to handle the tension (40 kg in each direction for the cathode wires for the full-size BetaCage) and can be precision machined when properly annealed. The field shapers can be made of acrylic, which is even cleaner.

The final design employs a Noryl frame manufactured as four arms that are then bolted together. The frame design is visible in Figure 4. The holes for the wire feedthroughs are centered with 10 μm precision, and the dimensions of the pieces meet tolerances of 125 μm. Two arms have holes for the anode wires, while the other two arms have holes for the crossed cathode-plane wires.

The holes accept brass feedthroughs modeled on those developed for the BaBar wire chambers, shown in Figure 7. The cylindrical outer dimension press fits into the holes in the Noryl, and they have a 100 μm hole (175 μm for the cathode wires) that centers the wire. A copper tube inserted into the other end of the brass pieces guides the wire into the feedthrough and is crimped to keep the wire in place. The wires are crimped into the feedthroughs under tension. Springs in the feedthroughs at one end of the wires are compressed in this process, maintaining tension in case the wires relax and also providing some compliance in case the wires are disturbed.

3.4 Readout Electronics

A full readout system must monitor, with time information, all the wires of the bulk MWPC anode and one of its crossed cathodes in order to reconstruct the track in three dimensions. This is not just a matter of measuring hit positions, though, because an electrical model reveals that the pulse shape depends on the position of an event along a particular wire at the 30% level (Figure 5). Since maintaining an energy resolution sufficient to identify beta-decay endpoints (or alpha energies) is critically important for the BetaCage, it is necessary to recover as much information about the pulse shape as possible to correct for these variations and reach the resolution limit imposed by counting statistics. This requires digitization at speeds approaching 1 GHz as well as full readout of the crossed cathode, which also provides position information.

It is not cost effective to read out each wire individually. In the veto and trigger MWPCs, we gang all the wires together since we do not need to reconstruct position there. We gang the edge wires of the bulk MWPC anode and cathode together to form veto regions, and we gang the remaining bulk wires together in a pseudo-random fashion. This latter ganging is chosen so that it is always possible to reconstruct which cells were hit by combining pulse shape information with the crossed-wire hit information. For the full-size BetaCage, we can divide the anode and cathode into 20 gangs of 8–10 wires per gang with 42 readout channels.

The readout system thus developed is as follows. The high voltage will be supplied by a board developed by our U. Alberta collaborators (D. Grant). At the vacuum feedthroughs to the chamber, we place front-end wideband voltage amplifiers consisting of two stages of the Mini-Circuits PSA-5454+ 50 MHz to 4 GHz low-noise MMIC amplifier followed by a 500-MHz cutoff anti-alias filter. These have been developed by U. Alberta also. These boards also serve to receive the high-voltage and connect it to the wires, with a blocking capacitor placed between the MWPC wires and the wideband amplifier chip. The amplified signals then enter a custom ADC board designed by Techne Instruments. Each board has six Texas Instruments ADS5400 1-GHz, 12-bit ADCs. The board mates to a ROACH[3] board, which has a Virtex-5 FPGA, a PowerPC CPU, and on-board memory. FPGA firmware pipes this output to an on-board FIFO buffer as well as to a low-pass filter followed by a discriminator, which provides a trigger. The trigger is disseminated to the remainder of the ADC/ROACH boards to command storage of the data, followed by readout of the buffers from the various boards by a DAQ computer.

The above design was analyzed using standard optimal filter theory and the energy resolution was calculated, as shown in Figure 5. The front-end amplifier contributes negligibly, at the level of 0.05 keV. The ADC quantization noise is a larger contribution, about 0.2 keV. Given a track length of roughly 30 cm for a 150-keV electron, the energy deposited per 5-mm MWPC cell is about 2.5 keV, and so the energy in a single cell can be detected with ample signal-to-noise of roughly 10. (Note that, while the statistical fluctuations on electron-ion pair creation degrade the energy resolution, they do not degrade the reconstruction of position along the wire, which is determined only by electronics noise.) The ADC full scale of 2 V corresponds to roughly 200 keV energy deposition.

3.5 Gas Handling

To ensure low backgrounds, it is especially important to limit the radon in the chamber. Radon may be emanated by materials and is present in the commercial Ne/CH_4 mix (formed from ultra-high purity neon and chemically pure methane) at small levels. To remove this radon, the gas-handling system includes a standard cooled, carbon radon trap (see *e.g.* [38]). While such a trap is fundamentally simple, care must be taken that the carbon itself has low radon emanation. Furthermore, the packing of the carbon must be as tight as possible to minimize channels through which radon may pass without adsorbing to the carbon. Our collaborator (R. Schnee, Syracuse) has acquired a suitable synthetic carbon, SARATECH by Blücher GmbH. This trap will also be effective at removing ^{85}Kr, a lesser background.

The cost of neon gas makes it cost-effective to recirculate the Ne/CH_4 mixture. We will use a

---

[3] An open-source platform designed by the Center for Astronomical Signal Processing and Electronics Research, `http://casper.berkeley.edu`, and commercially available.

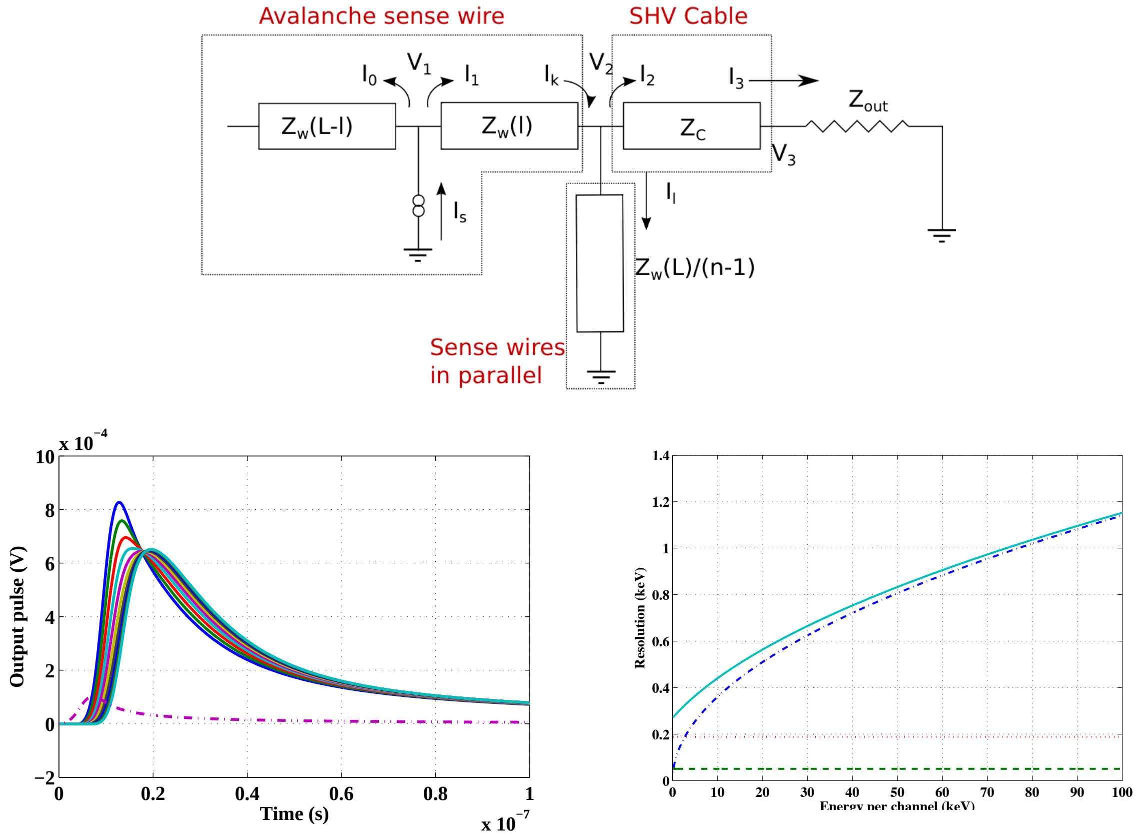

Figure 5: Top: Electrical model for BetaCage MWPC pulse shape. The avalanche event at a particular point along the wire acts as a current source I_s injecting current into the anode (sense) wire. That wire is treated as a transmission line formed by the anode wire and the nearby anode and cathode wires (characteristic impedance Z_w given by the capacitance to adjacent wires and the wire inductance and resistance). It is unterminated at one end and connects to a coaxial cable (impedance Z_c) and then to an amplifier (not shown) with input impedance Z_{out} at the other. The anode wires ganged together with this one appear as a shunt impedance to ground. Bottom left: Dependence of pulse height and shape on position in steps of 10% of the wire length for a 1-m wire. The small dot-dashed line is the input current pulse. The increase in pulse height is due to the gain of the amplifier, included in the model because its bandwidth affects the pulse shape. The 30% variation in peak height is due to the resistance of the anode wire, while the variation in pulse shape arises from the dependence of the effective R and C on the position of the event along the wire. Bottom right: Expected energy resolution as a function of input energy. The dashed-dotted line is the statistical fluctuations in number of charge pairs created, the dashed line is the noise of the analog component of the readout (thermal and amplifier noise), the dotted line is the digitization noise, and the solid line is the quadrature sum. Note that the statistical noise does not degrade the determination of pulse shape and position; it only comes in when converting from pulse height to energy.

KNF Neuberger N816 4–11 liter-per-minute, double-diaphragm pump. A SAES Pure Gas PS11-MC1-CH getter-stabilized zeolite gas purifier will remove water, CO_2, O_2, non-methane hydrocarbons, and particulates greater than 0.003 μm in size. The Ne/CH_4 mixture fraction should remain essentially constant for the days to weeks of counting between gas replacement since the event rate in the chamber will be low enough that dissociation of the methane is negligible. The gas-handling system design is shown in Figure 6.

4 Results

This DUSEL R&D grant (DE-FG02-07ER41481, \$172,000, 7/15/2007–7/14/2011), a companion DUSEL R&D grant to collaborator R. Schnee (Syracuse; Co-PI: Golwala; NSF/PHY-0834453;

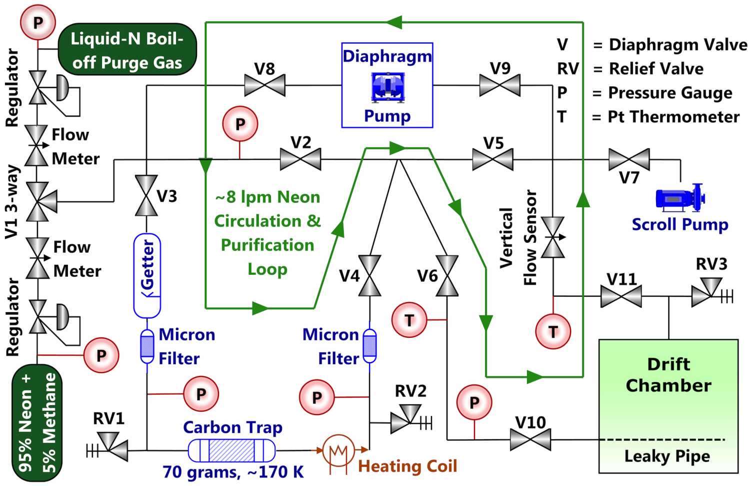

Figure 6: A schematic of the betacage gas handling system, with a purification loop reducing the Rn-induced background and other contaminants.

$200,841, 6/2007–5/2012), Schnee's startup, and Grant's Canadian funds supported the work leading to the design and to construction and testing of the prototype BetaCage, which is half the size of the full-size BetaCage in each dimension and has a drift volume of 41 cm× 41 cm × 22 cm. As described below, these tests have demonstrated many aspects of the detector design. We expect to demonstrate full track reconstruction by Fall, 2014. With these demonstrations in hand, doubling the size of the detector to the full-size BetaCage should pose no major design or implementation challenges.

This grant partially supported graduate student Zeeshan Ahmed, postdoc Robert Nelson, and four undergraduates. Ahmed received his Ph. D. in 2011 based on his design work for the BetaCage (and the analysis of CDMS II data). Nelson joined the project in August, 2010, taking over design and assembly work from Ahmed. He managed the demonstration of the ^{55}Fe testing of the MWPC design, supervising four undergraduates: Dan Sotolongo, who helped develop the stringing technique, strung the first MWPC and its prototype, and also developed the LABVIEW data acquisition; Sinthunon Chavanaves, who worked on GARFIELD simulations; Alex Rider, who worked on printed-circuit board design, wiring, and acquired and analyzed the data sets presented in Section 4.1; and Alex Zahn, who has worked on characterizing the BetaCage readout system and on developing firmware and software for readout. Both Rider and Zahn were granted Caltech Summer Undergraduate Research Fellowships for summer, 2012, and wrote senior undergraduate theses. Rider graduated in June, 2013, and is pursuing graduate studies at Stanford University. Nelson departed Caltech in August, 2013, to join Aerospace Corp. Zahn has stayed on for a year after graduation while applying to graduate school to complete the BetaCage readout and demonstrate track reconstruction.

This work has resulted in two conference proceedings [8, 9] and one paper accepted for publication in a refereed journal [39]. The paper is appended to the end of this report and fully describes the detailed design, assembly, and performance of the MWPCs described above. We summarize these results below and also discuss progress on the full readout electronics, track reconstruction algorithms, and background simulations not reported there.

4.1 MWPC Assembly and Performance

A clever assembly jig, shown in Figure 7, enables the stringing of a single wire in 6 minutes with good control of positioning, feedthrough insertion force, and tension. A full MWPC for the prototype,

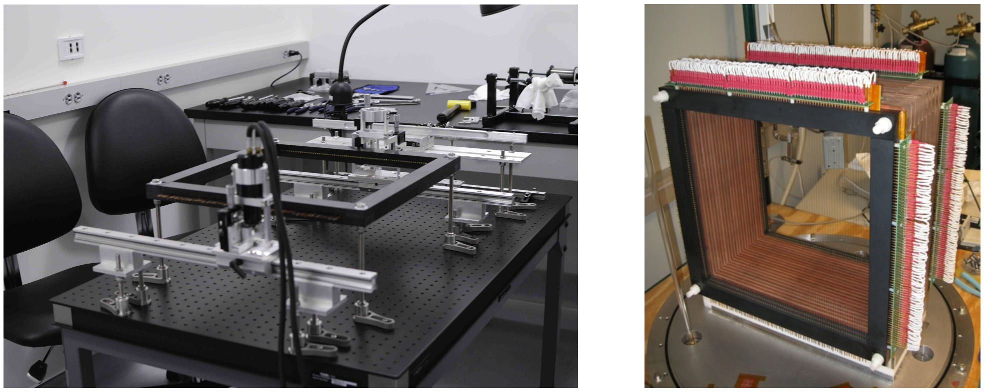

Figure 7: Left: Picture of assembly bench for MWPC stringing. From the front of the picture to the back: Spring-side crimper jig on a movable cart, Noryl MWPC frame, tension-side crimper jig on a movable cart, low-friction tensioning bar and pulley, wire spool (on tool bench). Right: Completed prototype, with two MWPCs and field shapers surrounding the drift region.

with 237 wires, was assembled in 5 days by 3 people in December, 2011. The two MWPCs for the prototype BetaCage are fully assembled, as shown in Figure 7.

We tested these MWPCs by exposing them to a collimated ^{55}Fe X-ray source, with lines at 5.89 (Mn K_α) and 6.49 (Mn K_β) keV. A Bertan Model 375 P high-voltage supply filtered with a two-stage low-pass filter with 72 Hz cutoff frequency held the anode at 2100 V and the cathodes at 100 V. A copper-clad sheet of G-10 was used to provide ground planes 10 mm from the cathodes. The anode wires were read out using a Cremat CR-111 two-stage charge-integrating amplifier with 0.13 V/pC gain, 150 μs decay time , and 3 ns intrinsic rise time. The output was digitized with a 60 MHz, 12-bit National Instruments PCI-5105 ADC. Because of high-frequency noise, we took data in a mode where we filled the board's memory with long, continuous traces and then, after downloading the buffer and in software, we applied a 10 kHz low-pass 6th-order Butterworth filter. We identified pulses in the filtered trace above a minimum peak height and used the filtered peak height to estimate energy.

The performance is excellent, as indicated by the spectrum shown in Figure 8, obtained after tuning the anode voltage to 2100 V to ensure good separation of the X-ray events from noise while avoiding saturation. The ^{55}Fe peak is readily visible, as is the argon K-shell "escape" peak (≈ 3 keV). Assuming the standard value of 26 eV deposited energy per electron-ion pair, we reconstruct that the MWPC gain is 10^4. The energy resolution at 6 keV is 15.8% FWHM estimated from a double-Gaussian fit to the two K-shell peaks. The statistical contribution is 14.2%, where the theoretical expectation is 12–13% based on Fano and avalanche statistics. The measure zero-pulse-height electronics noise contribution is only 2.2% FWHM, while the non-statistical contribution derived from the 6-keV spectrum is 7.6%. While the non-statistical contribution is appreciably larger than expected, this should not prove to be a limiter in practice. During typical operation for beta screening, the energy per 5-mm cell will be approximately 2.5 keV, at which energy the theoretical statistics-limited resolution will scale by $1/\sqrt{E}$ to approximately 22% FWHM, rendering any such non-statistical contribution, as well as the electronic noise, negligible. Furthermore, any such non-statistical and electronic noises will decrease with upgrades to the electronics, gas-handling system, and a position-corrected analysis, all discussed below.

From the dependence of the spectrum centroid on anode voltage, we verified the Diethorn parameters ($E_{\min}(\rho_0) = 48 \pm 3$ kV/cm and $\Delta V = 23.6 \pm 5.4$ V [40]), as shown in Figure 9. We also measured that the gain depends on gas pressure as $\delta G/G = -6.7\,\delta\rho/\rho$, consistent with expectations within the theoretical uncertainties, also shown in Figure 9.

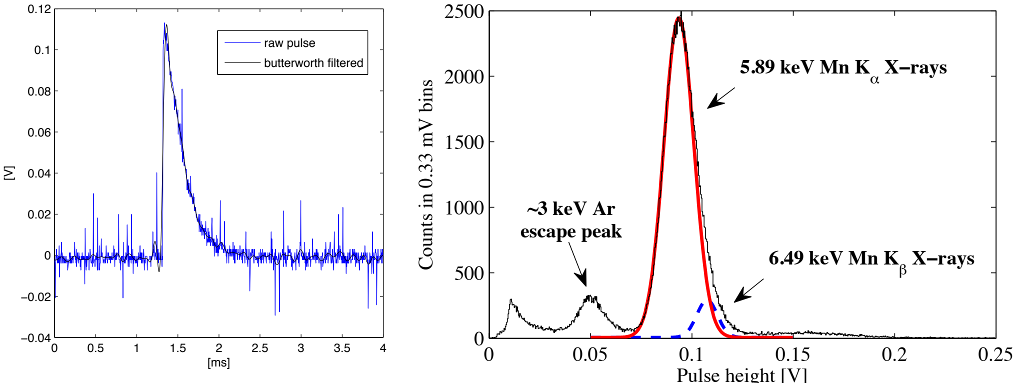

Figure 8: Left: A typical pulse for a ^{55}Fe-decay Mn X-ray event. The raw pulse exhibits high-frequency noise. A Butterworth filter applied in software removes this noise and provides a clean pulse. Center: Observed spectrum in MWPC in response to ^{55}Fe-decay Mn X-rays. The lower-energy peak is the argon escape peak. The spectrum is described in the text.

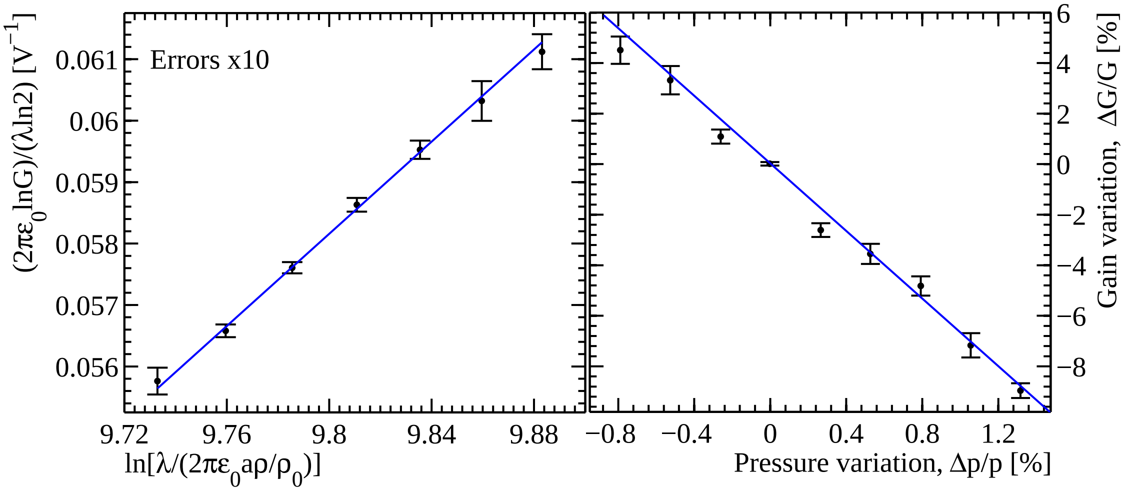

Figure 9: Left: Test of the Diethorn formula for gas gain in a proportional chamber, where Equation 1 has been rearranged to yield a linear relationship with varying anode voltage (dots with exaggerated 1σ error bars). An estimate of the Diethorn parameters is extracted with a linear fit; $\Delta V = 26.7 \pm 0.6\,\text{V}$ and $E_{\text{min}} = 38.3 \pm 1.3\,\text{kV/cm}$, in agreement with expectation. Right: gain variation, as measured with 5.89 keV X-rays, as a function of pressure change (dots with 1σ error bars). The Diethorn formula predicts a slope of -6.5 ± 0.3 that is confirmed by a best-fit slope of -6.7 ± 0.3.

Gas gain and overall system stability were measured from the mean value of the 6 keV peak as a function of time, which follows a bounded exponential form with amplitude $A = -2.8\%$ and time constant $\tau = 5.1$ h. This drift is negligible compared to the statistics-limited energy resolution at the 2.5 keV energy/cell level, but it may become noticeable in the reconstructured energy spectrum, which will go up to 200 keV.

4.2 Readout System Status

We have one copy of the Alberta HV supply in hand and are currently testing it with the Cremat readout so we can make a direct comparison to the data shown in Section 4.1, which was taken with a commercial Bertan HV supply.

We tested a prototype of the Alberta front-end amplifier on the bench. Its performance is shown in Figure 10. At high frequencies, above 50 MHz, its performance appears to be in good

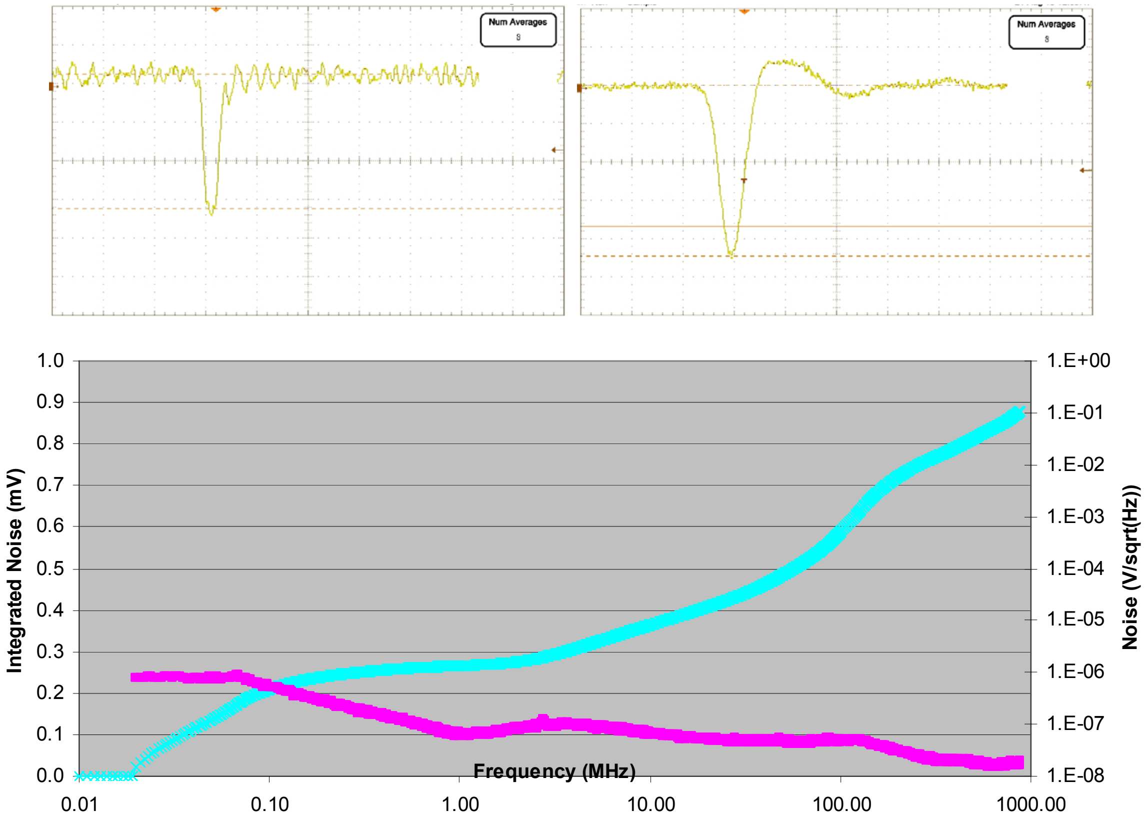

Figure 10: Top: Test of front-end amplifer. Top left: input pulse (2.5 ns/div, 2 mV/div). Top right: output pulse (2.5 ns/div, 100 mV/div). The ratio of output to input peak heights is 60. Bottom: noise power spectral density (logarithmic right axis) and integrated noise as a function of upper cutoff frequency (linear left axis). The noise from the front-end amplifier, Mini-Circuits PSA-5454+, referred to the output (as plotted in the figure) is expected to be 50 nV/Hz$^{-1/2}$ at 50 MHz and 25 nV/Hz$^{-1/2}$ at 500 MHz, in good agreement with the measurement.

agreement with expectations. The calculation of the electronics contribution to the total noise shown in Figure 5 assumes the noise is white with the 500 MHz value given in Figure 10. That assumption yields 0.05 keV rms contribution to the energy resolution and 0.5 mV rms noise at the amplifier output. Instead, we see the noise rises below 500 MHz, causing the total noise to be about 0.9 mV rms at the amplifier output. Given how subdominant the electronics noise is in Figure 5, this increase is not a concern. It can be mitigated somewhat by applying a high-pass filter at around 10 MHz, which preserves $\sim 90\%$ of the signal bandwidth (the pulse shape's 3 dB rolloff point is at about 100 MHz), but this would only reduce the noise to about 0.8 mV rms. Certainly, the amplifier's noise performance is acceptable as-is. The high-voltage supply adds no appreciable noise at the high frequencies of interest because it is aggressively low-pass filtered before it is sent to the wires. The Johnson noise of the HV bias resistors has already been incorporated in the noise budget.

We have a sufficient number of ADC and ROACH boards in hand for the full-size BetaCage and have been working on the firmware, data acquisition, and triggering. We are able to digitize signals with the ROACH boards and offload them to the DAQ computer. We have developed a very simple trigger (threshold trigger on a boxcar average of the incoming signal) and are working on using it to initiate storage of traces from all six ADCs as well as communication of the trigger to the other ROACH boards. We are increasing the sophistication of the on-board buffering so that

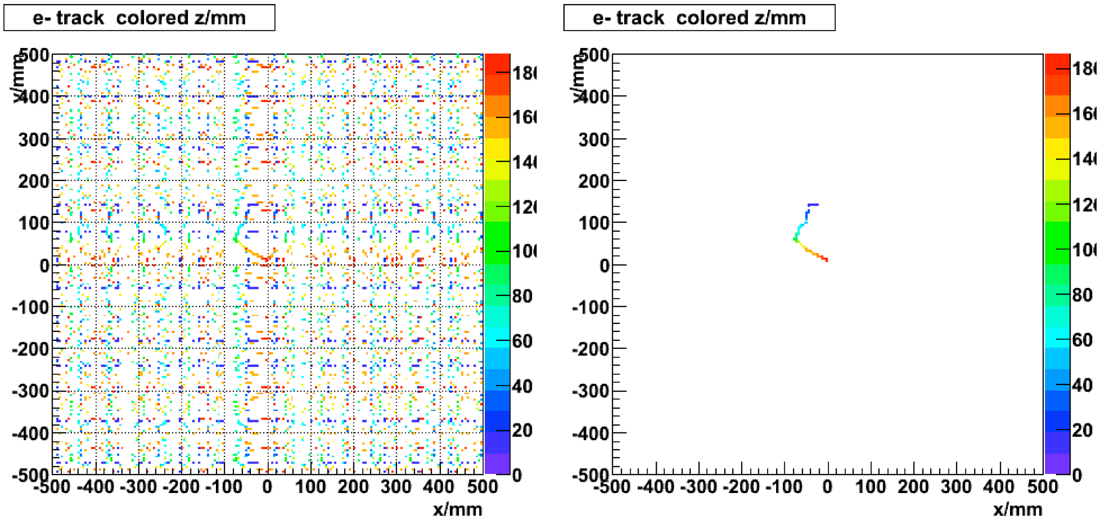

Figure 11: Left: Simulated raw hit information with pseudo-random groups of 10 wires read out together. The color scale indicates the z position of each energy deposition, as inferred by the drift time. The position of each dot in x and y indicates all possible wire combinations that may have been hit. Right: Inferred track path as found using the reconstruction algorithm.

the system can operate without dead time. There is sufficient on-board memory to allow this.

4.3 Track Reconstruction, Efficiency Determination, and Background Rejection

We devised an algorithm to reconstruct tracks given the pseudo-random wire ganging scheme mentioned earlier. We tested the algorithm using tracks created in GEANT4, as illustrated in Figure 11. We assigned the charge to MWPC cells of size 5 mm × 5 mm with z-resolution based on our expected timing resolution, combined signals from ganged wires, added electronics noise, and enforced a 0.8 keV threshold for deposited energy in each cell, in order to have a negligible fraction of hits solely due to noise fluctuations. This threshold energy results in some cells of the particle's track being mistakenly considered below threshold. For each wire "hit," the algorithm makes a list of unit cells the hit could be assigned to given the anode and cathode wires and timing. It then takes the hit closest to the sample and sees which of its nearest-neighbor candidates have a hit. It then tries to find adjacent hits for those secondary hits found. The process is repeated until the set of cells connected to the first hit is found. The process is repeated starting at other hit cells not yet included in the set, and all the sets are ranked by size. Then sets are merged if they are within 2 empty cells of each other and do not include many common cells. The algorithm works well except in rare cases when tracks move horizontally, producing many hit cells with the same z value.

We also simulated the efficiency for full containment of a track in the fiducial region for the prototype and full-size BetaCage, as shown in Figure 12. The full size BetaCage loses efficiency above 100 keV as one moves out from the center of the fiducial region, but it remains acceptable. The larger efficiency loss is from electrons that terminate back on the sample before losing their full energy. These will be easily identified via the track image. The prototype BetaCage is of course less efficient with neon gas, but that is not a concern as it will be used with a high-rate source for testing, and the primarily goal of neon operation for the prototype is to test drift gas properties, not take low-rate data. Alpha screening data with the prototype will be taken with P10, for which the efficiency will be higher.

We have also simulated the effectiveness with which track reconstruction can be used to reject

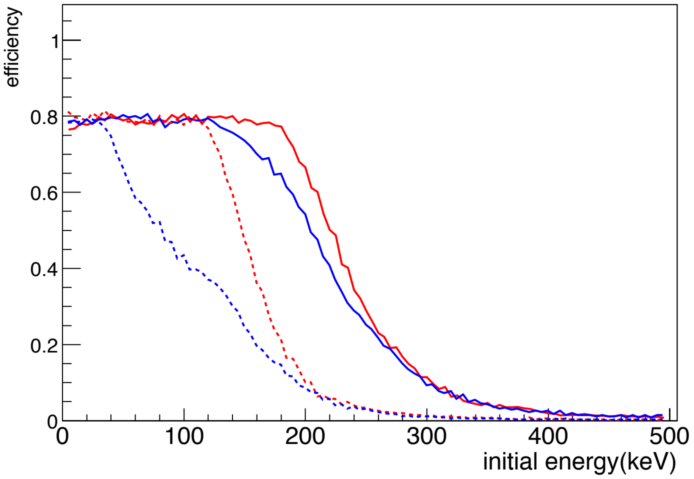

Figure 12: Left: Efficiency for containment of events in the BetaCage. An event originating in the sample under the fiducial section of the trigger grid can be lost if it enters the veto region, or if the electron suffers a large deflection and returns to the sample, depositing less than its full energy in the drift region. Shown is the fraction of events fully contained in fiducial region as a function of energy for the full-size BetaCage (solid) and the prototype running neon (dashed), for a source at the center (red) or 20 cm from the center (blue) of the fiducial region. The prototype BetaCage will be primarily run with P10, for which the efficiency will be higher; neon operation will be used primarily to test the drift properties of Ne/CH_4 mixtures.

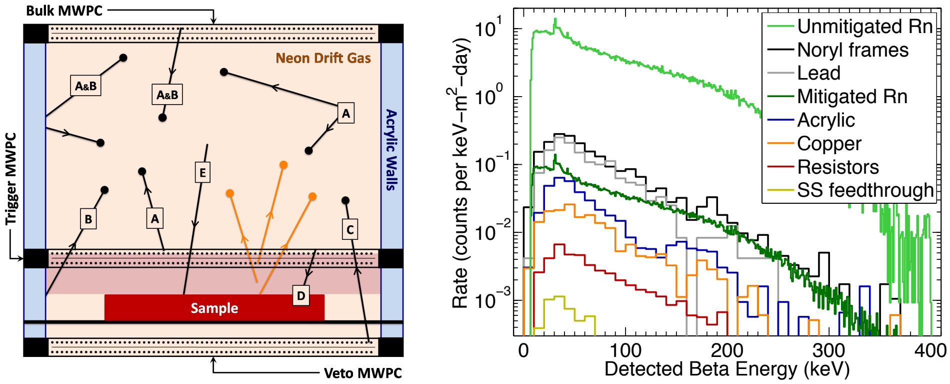

Figure 13: Left: Potential sources of backgrounds in the BetaCage. A number of track morphologies can be easily rejected (dark lines) by their (A) insufficient energy in the trigger MWPC, (B) lack of containment in the fiducial drift region, (C) too much energy in the veto MWPC, (D) insufficient energy in the bulk MWPC, or (E) uniform dE/dx, even at the apparent track end. Rejection is less effective (light lines) for betas or alphas emitted from the drift gas and cathode wires directly above the sample, or from the surface of the sample itself, following Rn-daughter implantation or Compton scattering. Right: expected backgrounds after all data-selection cuts, by source. The background from radon emanation (narrow-binned light green histogram) dominates unless it is mitigated (narrow-binned dark green histogram), as described in Section 3.5. From top to bottom, wide-binned spectra are from photons due to contamination in the Noryl MWPC frames, lead shielding, acrylic chamber, copper liner, field-shaping resistors, and stainless-steel feedthrough.

backgrounds. Figure 13 shows the multiple background sources we considered and the expected background levels expected, as previously summarized in Table 2. We see that, with appropriate mitigation of radon emanation using the gas-handling system (Section 3.5), the dominant backgrounds are from the Noryl frames and the lead shield.

5 Plans for the Prototype BetaCage and the Full BetaCage

There are two tasks remaining to commission the prototype BetaCage.

The first is to validate the amplifier design we have received from U. Alberta so that it can be produced for all the channels. As discussed in Section 4.2, we believe the noise PSD is acceptable, but we need to repeat the X-ray source test with the amplifier and fast readout electronics to verify statistics-limited resolution at 6 keV with the new electronics to be convinced of this. The firmware upgrade being undertaken to reduce the dead time is necessary for this test.

The second is to demonstrate full track reconstruction using a beta source emitting into the drift region using the techniques demonstrated via simulations in Section 4.3. For this measurement, we need to have the fast readout system set up to provide triggers between ROACH boards and also to have the DAQ read out multiple boards. Track reconstruction will also test the electron drift speed and electron diffusion in P10.

With the prototype fully commissioned, we will both undertake the engineering measurements on neon needed for the full-size BetaCage (Diethorn relation parameters, electron drift speed and diffusion, variation between 10% and 5% methane) as well as begin testing sensitivity for alpha screening. The detector can be available for alpha screening as soon as the sensitivity is understood.

These remaining efforts require primarily manpower (the amplifiers and HV supplies will be provided by U. Alberta) and some small amount of M&S funding, at the level of a few $k. The effort to completely commission the prototype will be supported by Golwala's DOE HEP base grant and Schnee's NSF PHY/PNA base grant. As noted above, the goal is to demonstrate full track reconstruction by Fall, 2014, so the prototype can be put into full operation for neon tests and alpha screening.

Collaborator R. Schnee is seeking opportunities to propose for funding for construction and commissioning of the full-size, radiopure BetaCage. The full-size BetaCage will be constructed in his radon-abated cleanroom at Syracuse. As noted earlier, a gas-handling system for the full-size BetaCage has been designed; purchase awaits funding. The primary other remaining items required are the detailed design of the shield, containment vessel, and load lock for the full BetaCage.

References

[1] B. Sadoulet, E. Beier, C. Fairhurst, T. Onstott, H. Robertson, and J. Tiedje, *A U.S. Deep Underground Science and Engineering Laboratory*, a proposal to NSF, submitted September, 2004, `http://www.dusel.org/S1Proposal_Final/DUSELProposal1.pdf`.

[2] P. Cushman and H. Miley, "Low-Level Counting Infrastructure and Requirements," in *A U.S. Deep Underground Science and Engineering Laboratory*, a proposal to NSF, supplementary materials, submitted September, 2004, `http://www.dusel.org//TechnicalDocumentsl/Final/lowlevelcounting_final.pdf`.

[3] P. Cushman and H. Miley, Report of the DUSEL Working Group on Low Background Counting Facilities and Prototyping for the NSF S1 Solicitation White Paper.

[4] P. Cushman, C. Galbiati, D. N. McKinsey, H. Robertson, T. M. P. Tait, D. Bauer, A. Borgland, B. Cabrera, F. Calaprice, J. Cooley, T. Empl, R. Essig, E. Figueroa-Feliciano, R. Gaitskell, S. Golwala, J. Hall, R. Hill, A. Hime, E. Hoppe, L. Hsu, E. Hungerford, R. Jacobsen, M. Kelsey, R. F. Lang, W. H. Lippincott, B. Loer, S. Luitz, V. Mandic, J. Mardon, J. Maricic, R. Maruyama, R. Mahapatra, H. Nelson, J. Orrell, K. Palladino, E. Pantic, R. Partridge, A. Ryd, T. Saab, B. Sadoulet, R. Schnee, W. Shepherd, A. Sonnenschein, P. Sorensen, M. Szydagis, T. Volansky, M. Witherell, D. Wright, and K. Zurek, "Snowmass CF1 Summary: WIMP Dark Matter Direct Detection," hep-ex/1310.8327, 2013.

[5] J. Cooley, P. Cushman, E. W. Hoppe, J. L. Orrell, and R. W. Schnee, "Low Background Materials and Assay - A Supplement to the Cosmic Frontier CF1 Summary," hep-ex/1311.3311, 2013.

[6] T. Shutt, C. E. Dahl, L. de Viveiros, R. J. Gaitskell, and R. W. Schnee, "Beta Cage: A New, Large-Area Multi-Wire Screening Detector For Surface Beta Contamination," in *Topical Workshop on Low Radioactivity Techniques: LRT 2004*, Vol. 785 of *American Institute of Physics Conference Proceedings* (American Institute of Physics, Melville, NY, 2005), pp. 79–83.

[7] R. W. Schnee, Z. Ahmed, S. R. Golwala, D. R. Grant, and K. Poinar, "Screening Surface Contamination with BetaCage," in *Topical Workshop on Low Radioactivity Techniques: LRT 2006*, Vol. 897 of *American Institute of Physics Conference Proceedings* (American Institute of Physics, Melville, NY, 2007), pp. 20–25.

[8] Z. Ahmed, S. R. Golwala, D. R. Grant, M. Kos, R. H. Nelson, R. W. Schnee, and B. Wang, "Status of BetaCage: an Ultra-sensitive Screener for Surface Contamination," in *Topical Workshop on Low Radioactivity Techniques: LRT 2010*, Vol. 1338 of *American Institute of Physics Conference Series*, edited by R. Ford (American Institute of Physics, Melville, NY, 2011), pp. 88–92.

[9] R. Bunker, Z. Ahmed, M. A. Bowles, S. R. Golwala, D. R. Grant, M. Kos, R. H. Nelson, R. W. Schnee, A. Rider, B. Wang, and A. Zahn, "The BetaCage, an ultra-sensitive screener for surface contamination," in *Topical Workshop on Low Radioactivity Techniques: LRT 2013*, Vol. 1549 of *American Institute of Physics Conference Proceedings*, edited by L. Miramonti and L. Pandola (American Institute of Physics, Melville, NY, 2013), pp. 132–135.

[10] Z. Ahmed, D. S. Akerib, S. Arrenberg, C. N. Bailey, D. Balakishiyeva, L. Baudis, D. A. Bauer, P. L. Brink, T. Bruch, R. Bunker, B. Cabrera, D. O. Caldwell, J. Cooley, P. Cushman, M. Daal,

F. DeJongh, M. R. Dragowsky, L. Duong, S. Fallows, E. Figueroa-Feliciano, J. Filippini, M. Fritts, S. R. Golwala, D. R. Grant, J. Hall, R. Hennings-Yeomans, S. A. Hertel, D. Holmgren, L. Hsu, M. E. Huber, O. Kamaev, M. Kiveni, M. Kos, S. W. Leman, R. Mahapatra, V. Mandic, K. A. McCarthy, N. Mirabolfathi, D. Moore, H. Nelson, R. W. Ogburn, A. Phipps, M. Pyle, X. Qiu, E. Ramberg, W. Rau, A. Reisetter, T. Saab, B. Sadoulet, J. Sander, R. W. Schnee, D. N. Seitz, B. Serfass, K. M. Sundqvist, M. Tarka, P. Wikus, S. Yellin, J. Yoo, B. A. Young, and J. Zhang, "Dark Matter Search Results from the CDMS II Experiment," *Science* **327**, 1619–1621 (2010).

[11] EDELWEISS Collaboration, E. Armengaud, C. Augier, A. Benoît, L. Bergé, J. Blümer, A. Broniatowski, V. Brudanin, B. Censier, G. Chardin, M. Chapellier, F. Charlieux, P. Coulter, G. A. Cox, X. Defay, M. de Jesus, Y. Dolgorouki, J. Domange, L. Dumoulin, K. Eitel, D. Filosofov, N. Fourches, J. Gascon, G. Gerbier, J. Gironnet, M. Gros, S. Henry, S. Hervé, A. Juillard, H. Kluck, V. Kozlov, H. Kraus, V. A. Kudryavtsev, P. Loaiza, S. Marnieros, X.-F. Navick, C. Nones, E. Olivieri, P. Pari, L. Pattavina, B. Paul, M. Robinson, S. Rozov, V. Sanglard, B. Schmidt, S. Scorza, S. Semikh, A. S. Torrento-Coello, L. Vagneron, M.-A. Verdier, R. J. Walker, and E. Yakushev, "Final results of the EDELWEISS-II WIMP search using a 4-kg array of cryogenic germanium detectors with interleaved electrodes," *Phys. Lett. B* **702**, 329–335 (2011).

[12] Y. D. Kim for the XMASS Collaboration, "The Status and Background Considerations of XMASS Experiment," in *Topical Workshop on Low Radioactivity Techniques: LRT 2006*, Vol. 897 of *American Institute of Physics Conference Proceedings* (American Institute of Physics, Melville, NY, 2007), pp. 79–84.

[13] A. Takeda for the XMASS Collaboration, "Low background techniques in XMASS," in *Topical Workshop on Low Radioactivity Techniques: LRT 2010*, Vol. 1338 of *American Institute of Physics Conference Proceedings* (American Institute of Physics, Sudbury, Canada, 2011), pp. 123–125.

[14] R. Ardito, C. Arnaboldi, D. R. Artusa, F. T. Avignone, M. Balata, I. Bandac, M. Barucci, J. W. Beeman, F. Bellini, C. Brofferio, C. Bucci, S. Capelli, F. Capozzi, L. Carbone, S. Cebrian, M. Clemenza, C. Cosmelli, O. Cremonesi, R. J. Creswick, I. Dafinei, A. de Waard, M. Diemoz, M. Dolinski, H. A. Farach, F. Ferroni, E. Fiorini, S. J. Freedman, G. Frossati, C. Gargiulo, A. Giuliani, P. Gorla, E. Guardincerri, T. D. Gutierrez, E. E. Haller, K. M. Heeger, I. G. Irastorza, E. Longo, R. Maruyama, S. Morganti, S. Nisi, C. Nones, E. B. Norman, A. Nucciotti, N. Xu, E. Olivieri, P. Ottonello, M. Pallavicini, E. Palmieri, M. Pavan, M. Pedretti, G. Pessina, S. Pirro, E. Previtali, L. Risegari, C. Rosenfeld, S. Sangiorgio, M. Sisti, A. R. Smith, L. Torres, G. Ventura, and L. Zanotti, "The CUORICINO and CUORE double beta decay experiments," *Prog. Part. Nucl. Phys.* **57**, 203–216 (2006).

[15] F. Alessandria, E. Andreotti, R. Ardito, C. Arnaboldi, F. T. Avignone, M. Balata, I. Bandac, T. I. Banks, G. Bari, J. Beeman, F. Bellini, A. Bersani, M. Biassoni, T. Bloxham, C. Brofferio, A. Bryant, C. Bucci, X. Z. Cai, L. Canonica, S. Capelli, L. Carbone, L. Cardani, M. Carrettoni, N. Chott, M. Clemenza, C. Cosmelli, O. Cremonesi, R. J. Creswick, I. Dafinei, A. Dally, A. De Biasi, M. P. Decowski, M. M. Deninno, A. de Waard, S. Di Domizio, L. Ejzak, R. Faccini, D. Q. Fang, H. A. Farach, E. Ferri, F. Ferroni, E. Fiorini, L. Foggetta, S. J. Freedman, G. Frossati, A. Giachero, L. Gironi, A. Giuliani, P. Gorla, C. Gotti, E. Guardincerri, T. D. Gutierrez, E. E. Haller, K. Han, K. M. Heeger, H. Z. Huang, K. Ichimura, R. Kadel, K. Kazkaz, G. Keppel, L. Kogler, Y. G. Kolomensky, S. Kraft, D. Lenz, Y. L. Li, X. Liu, E. Longo, Y. G. Ma, C.

Maiano, G. Maier, C. Martinez, M. Martinez, R. H. Maruyama, N. Moggi, S. Morganti, S. Newman, S. Nisi, C. Nones, E. B. Norman, A. Nucciotti, F. Orio, D. Orlandi, J. L. Ouellet, M. Pallavicini, V. Palmieri, L. Pattavina, M. Pavan, M. Pedretti, G. Pessina, S. Pirro, E. Previtali, V. Rampazzo, F. Rimondi, C. Rosenfeld, C. Rusconi, C. Salvioni, S. Sangiorgio, D. Schaeffer, N. D. Scielzo, M. Sisti, A. R. Smith, F. Stivanello, L. Taffarello, G. Terenziani, W. D. Tian, C. Tomei, S. Trentalange, G. Ventura, M. Vignati, B. S. Wang, H. W. Wang, C. A. Whitten, T. Wise, A. Woodcraft, N. Xu, L. Zanotti, C. Zarra, B. X. Zhu, and S. Zucchelli, “CUORE crystal validation runs: Results on radioactive contamination and extrapolation to CUORE background,” *Astropart. Phys.* **35**, 839–849 (2012).

[16] J. A. Nikkel, W. H. Lippincott, and D. N. McKinsey, “Neutrino and dark matter detection with CLEAN,” *Int. J. Mod. Phys. A* **20**, 3113–3114 (2005).

[17] B. Cai, M. Boulay, B. Cleveland, and T. Pollmann, “Surface backgrounds in the DEAP-3600 dark matter experiment,” in *Topical Workshop on Low Radioactivity Techniques: LRT 2010*, Vol. 1338 of *American Institute of Physics Conference Series*, edited by R. Ford (American Institute of Physics, Melville, NY, 2011), pp. 137–146.

[18] L. Bond, J. I. Collar, J. Ely, M. Flake, J. Hall, D. Jordan, D. Nakazawa, A. Raskin, A. Sonnenschein, and K. O. Sullivan, “Development of bubble chambers with sensitivity to WIMPs,” *New Astron. Rev.* **49**, 271–275 (2005).

[19] W. J. Bolte, J. I. Collar, M. Crisler, J. Hall, J. Krider, K. Crum, D. Holmgren, C. M. Lei, D. Nakazawa, H. Nguyen, B. Odom, K. O’Sullivan, R. Plunkett, E. Ramberg, A. Raskin, J. Rasmussen, R. Schmitt, A. Sonnenschein, M. Szydagis, and J. D. Vieira, “A bubble chamber for dark matter detection (the COUPP project status),” *J. Phys. Conf. Ser.* **39**, 126–128 (2006).

[20] E. Aprile and XENON1T collaboration, “The XENON1T Dark Matter Search Experiment,” astro-ph.IM/1206.6288, 2012.

[21] D. C. Malling, D. S. Akerib, H. M. Araujo, X. Bai, S. Bedikian, E. Bernard, A. Bernstein, A. Bradley, S. B. Cahn, M. C. Carmona-Benitez, D. Carr, J. J. Chapman, K. Clark, T. Classen, T. Coffey, A. Curioni, A. Currie, S. Dazeley, L. de Viveiros, M. Dragowsky, E. Druszkiewicz, C. H. Faham, S. Fiorucci, R. J. Gaitskell, K. R. Gibson, C. Hall, M. Hanhardt, B. Holbrook, M. Ihm, R. G. Jacobsen, L. Kastens, K. Kazkaz, R. Lander, N. Larsen, C. Lee, D. Leonard, K. Lesko, A. Lindote, M. I. Lopes, A. Lyashenko, P. Majewski, R. Mannino, D. N. McKinsey, D. . Mei, J. Mock, M. Morii, A. S. J. Murphy, H. Nelson, F. Neves, J. A. Nikkel, M. Pangilinan, P. Phelps, L. Reichhart, T. Shutt, C. Silva, W. Skulski, V. Solovov, P. Sorensen, J. Spaans, T. Stiegler, T. J. Sumner, R. Svoboda, M. Sweany, M. Szydagis, J. Thomson, M. Tripathi, J. R. Verbus, N. Walsh, R. Webb, J. T. White, M. Wlasenko, F. L. H. Wolfs, M. Woods, and C. Zhang, “After LUX: The LZ Program,” astro-ph.IM/1110.0103, 2011.

[22] A. Wright for the DArkSIDE Collaboration, “The DArkSIDE Program at LNGS,” phys.ins-det/1109.2979v1, 2011.

[23] A. J. Da Silva, “Development of a low background environment for the cryogenic dark matter search,” Ph.D. thesis, University of British Columbia, 1996.

[24] D. Abrams, D. S. Akerib, M. S. Armel-Funkhouser, L. Baudis, D. A. Bauer, A. Bolozdynya, P. L. Brink, R. Bunker, B. Cabrera, D. O. Caldwell, J. P. Castle, C. L. Chang, R. M. Clarke,

M. B. Crisler, R. Dixon, D. Driscoll, S. Eichblatt, R. J. Gaitskell, S. R. Golwala, E. E. Haller, J. Hellmig, D. Holmgren, M. E. Huber, S. Kamat, A. Lu, V. Mandic, J. M. Martinis, P. Meunier, S. W. Nam, H. Nelson, T. A. Perera, M. C. Perillo Isaac, W. Rau, R. R. Ross, T. Saab, B. Sadoulet, J. Sander, R. W. Schnee, T. Shutt, A. Smith, A. H. Sonnenschein, A. L. Spadafora, G. Wang, S. Yellin, and B. A. Young, "Exclusion limits on the WIMP-nucleon cross section from the Cryogenic Dark Matter Search," *Phys. Rev. D* **66**, 122003/1–35 (2002).

[25] P. Vojtyla, "Fast computer simulations of background of low-level Ge γ-spectrometers induced by ^{210}Pb/^{210}Bi in shielding lead," *Nucl. Instrum. Meth. B* **117**, 189–198 (1996).

[26] D. N. McKinsey and K. J. Coakley, "Neutrino detection with CLEAN," *Astropart. Phys.* **22**, 355–368 (2005).

[27] C. Arpesella, H. O. Back, M. Balata, T. Beau, G. Bellini, J. Benziger, S. Bonetti, A. Brigatti, C. Buck, B. Caccianiga, L. Cadonati, F. Calaprice, G. Cecchet, M. Chen, O. Dadoun, D. D'Angelo, A. De Bari, A. de Bellefon, E. De Haas, H. de Kerret, A. Derbin, M. Deutsch, A. Di Credico, F. Elisei, A. Etenko, F. von Feilitzsch, R. Fernholz, R. Ford, D. Franco, B. Freudiger, C. Galbiati, F. Gatti, S. Gazzana, M. G. Giammarchi, D. Giugni, M. Göger-Neff, T. Goldbrunner, A. Golubchikov, A. Goretti, C. Grieb, C. Hagner, T. Hagner, W. Hampel, E. Harding, F. X. Hartmann, R. von Hentig, G. Heusser, M. Hult, A. Ianni, A. M. Ianni, J. Kiko, T. Kirsten, M. Köhler, G. Korga, G. Korschinek, Y. Kozlov, D. Kryn, P. LaMarche, M. Laubenstein, C. Lendvai, F. Loeser, P. Lombardi, K. McCarty, I. Machulin, S. Malvezzi, J. Maneira, I. Manno, G. Manuzio, A. Martemianov, F. Masetti, U. Mazzucato, E. Meroni, L. Miramonti, M. E. Monzani, P. Musico, H. Neder, L. Niedermeier, S. Nisi, L. Oberauer, M. Obolensky, F. Ortica, M. Pallavicini, L. Papp, L. Perasso, A. Pocar, R. S. Raghavan, G. Ranucci, W. Rau, A. Razeto, E. Resconi, T. Riedel, A. Sabelnikov, C. Salvo, R. Scardaoni, S. Schönert, K. H. Schuhbeck, T. Shutt, H. Simgen, A. Sonnenschein, O. Smirnov, A. Sotnikov, M. Skorokhvatov, S. Sukhotin, V. Tarasenkov, R. Tartaglia, G. Testera, P. R. Trincherini, V. Vyrodov, R. B. Vogelaar, D. Vignaud, S. Vitale, M. Wójcik, O. Zaimidoroga, and G. Zuzel, "Measurements of extremely low radioactivity levels in BOREXINO," *Astropart. Phys.* **18**, 1–25 (2002).

[28] G. Zuzel and M. Wójcik, "Removal of the long-lived ^{222}Rn daughters from copper and stainless steel surfaces," *Nucl. Instrum. Meth. A* **676**, 140–148 (2012).

[29] R. W. Schnee, M. A. Bowles, R. Bunker, K. McCabe, J. White, P. Cushman, M. Pepin, and V. E. Guiseppe, "Removal of long-lived ^{222}Rn daughters by electropolishing thin layers of stainless steel," in *Topical Workshop on Low Radioactivity Techniques: LRT 2013*, Vol. 1549 of *American Institute of Physics Conference Proceedings*, edited by L. Miramonti and L. Pandola (American Institute of Physics, Melville, NY, 2013), pp. 128–131.

[30] R. W. Schnee, R. Bunker, G. Ghulam, D. Jardin, M. Kos, and A. S. Tenney, "Construction and measurements of a vacuum-swing-adsorption radon-mitigation system," in *Topical Workshop on Low Radioactivity Techniques: LRT 2013*, Vol. 1549 of *American Institute of Physics Conference Proceedings*, edited by L. Miramonti and L. Pandola (American Institute of Physics, Melville, NY, 2013), pp. 116–119.

[31] R. P. Beukens, *Annual Report, IsoTrace Laboratory, Canadian Centre for Accelerator Mass Spectroscopy at the University of Toronto* (University of Toronto, Toronto, 1992).

[32] G. Bonvicini, N. Harris, and V. Paolone, “The chemical history of ^{14}C in deep oilfields,” hep-ex/0308025, 2003.

[33] J. Porstendorfer and T. T. Mercer, “Influence of electric charge and humidity upon the diffusion coefficient of radon decay products,” *Health Physics* **37**, 191–199 (1979).

[34] S. K. Dua, P. Kotrappa, and P. C. Gupta, “Influence of relative humidity on the charged fraction of decay products of radon and thoron,” *Health Physics* **45**, 152–157 (1983).

[35] S. Burgos, J. Forbes, C. Ghag, M. Gold, V. A. Kudryavtsev, T. B. Lawson, D. Loomba, P. Majewski, D. Muna, A. S. Murphy, G. G. Nicklin, S. M. Paling, A. Petkov, S. J. S. Plank, M. Robinson, N. Sanghi, N. J. T. Smith, D. P. Snowden-Ifft, N. J. C. Spooner, T. J. Sumner, J. Turk, and E. Tziaferi, “Track reconstruction and performance of DRIFT directional dark matter detectors using alpha particles,” *Nucl. Instrum. Meth. A* **584**, 114–128 (2008).

[36] W. K. Warburton and B. Dwyer-McNally, “Electronic background rejection in a new ultra-low background alpha-particle counter,” *Nucl. Instrum. Meth. B* **263**, 211–224 (2007).

[37] W. Blum and L. Rolandi, *Particle Detection with Drift Chambers* (Springer-Verlag, Berlin, 1993).

[38] H. Simgen and G. Zuzel, “Analysis of the 222rn concentration in argon and a purification technique for gaseous and liquid argon,” *Appl. Rad. and Isot.* **67**, 922–925 (2009).

[39] Z. Ahmed, M. A. Bowles, R. Bunker, S. R. Golwala, D. R. Grant, M. Kos, R. H. Nelson, A. Rider, R. W. Schnee, D. Sotolongo, B. Wang, and A. Zahn, “A prototype low-background multiwire proportional chamber for measuring alphas and low-energy betas,” physics.ins-det/1307.6154, 2013, accepted for publication in *J. Inst.*

[40] R. W. Hendricks, “The gas amplification factor in xenon-filled proportional counters,” *Nucl. Instrum. Meth. A* **102**, 309–312 (1972).

Preprint typeset in JINST style - HYPER VERSION

arXiv:1307.6154v2 [physics.ins-det] 25 Nov 2013

A prototype low-background multiwire proportional chamber

Z. Ahmed[a], **M. A. Bowles**[b], **R. Bunker**[b], **S. R. Golwala**[a], **D. R. Grant**[c], **M. Kos**[b],
R. H. Nelson[a]*, **A. Rider**[a], **R. W. Schnee**[b], **D. Sotolongo**[a], **B. Wang**[b], **and A. Zahn**[a]

[a]*Division of Physics, Math, and Astronomy*
California Institute of Technology
Pasadena, CA 91125, USA
[b]*Department of Physics*
Syracuse University
Syracuse, NY 13244, USA
[c]*University of Alberta*
Edmonton, AB, T6G 2R3, Canada
E-mail: `rhn@caltech.edu`

ABSTRACT: A prototype multiwire proportional chamber (MWPC) was developed to demonstrate the feasibility of constructing a radiopure time projection chamber with MWPC track readout to assay materials for alpha- and beta-emitting surface contaminants for future rare-event-search experiments as well as other scientific fields. The design features and assembly techniques described here are motivated by the position and energy resolution required to reconstruct alpha and beta tracks while efficiently rejecting backgrounds. Results from a test setup using an ^{55}Fe x-ray source indicate excellent operational stability and a near-ideal energy resolution of 15.8% FWHM at 5.89 keV and a gas gain of $\sim 10^4$.

KEYWORDS: electron multipliers (gas), wire chambers, particle tracking detectors (gaseous detectors), time projection chambers (TPC).

---

*Corresponding author.

Contents

1. Introduction

Future rare-event searches require unprecedented levels of radiopurity (see *e.g.* [1]). In particular, a troublesome source of contamination results from the noble-gas radioisotope ^{222}Rn, which is sufficiently long lived to pervade laboratory spaces and can lead to the implantation of its long-lived ^{210}Pb and ^{210}Po daughters into or near sensitive detector surfaces. Unfortunately, high-sensitivity detection of the ^{210}Pb 46 keV gamma ray from material surfaces is generally not feasible with HPGe detectors, in part due to its low branching fraction. Furthermore, since these surface contaminants are chemically separated and hence out of equilibrium with the photon-emitting isotopes in the parent ^{238}U decay chain, direct detection of the ^{210}Po alphas or betas from ^{210}Pb or ^{210}Bi is necessary to establish the surface contamination level. Detection of surface betas is necessary for isotopes that can be detected only by the betas they emit (*e.g.*, ^{3}H, ^{14}C, ^{32}Si, ^{63}Ni, ^{90}Sr, ^{106}Ru, ^{113m}Cd, ^{147}Pm, ^{151}Sm, ^{171}Tm, ^{194}Os, and ^{204}Tl). In addition to its importance for future rare-event searches, more sensitive detection of beta- and alpha-emitting surface contaminants would also benefit archeology, biology, climatology, environmental science, geology, integrated-circuit quality control, and planetary science [2].

A screener intended for low-background detection of alpha and low-energy beta decays has several stringent design requirements:

1. A high-efficiency detection mechanism with good sensitivity to non-penetrating particles from sample surfaces (*e.g.*, a 50 keV beta);
2. A low energy threshold to maximize detection rates from isotopes that emit primarily low-energy betas (*e.g.*, ^{210}Pb);
3. Sufficient energy resolution to permit identification of beta-emitting isotopes by their corresponding beta-spectrum endpoints and of isotopes that emit alphas, internal conversion electrons, or Auger electrons by their characteristic lines;
4. Sufficient position information to allow efficient identification of the source location of contamination and rejection of detector or external backgrounds (*i.e.*, fiducialization);
5. A well-shielded installation to reduce any external backgrounds that cannot be otherwise rejected; and
6. Clean construction from radiopure materials to minimize intrinsic backgrounds.

To achieve these goals, a gaseous time-projection chamber (TPC) is an ideal candidate. Placing a sample directly in the detection medium allows for $\sim 2\pi$ acceptance and very low energy thresholds as there is no dead layer (fulfilling requirements 1 and 2 above). A multiwire proportional chamber [3] (MWPC) has sufficient position and energy resolution for imaging the ionized particle tracks when drifted across the chamber (allowing requirements 3 and 4 to be fulfilled). Passive shielding (requirement 5) of the TPC is reasonably straightforward, and gases may be made sufficiently pure of intrinsic contaminants (partially fulfilling requirement 6). These considerations led to the design of a TPC called the BetaCage [4, 2, 5] with one MWPC near the sample to allow tagging of tracks starting from the sample, separated from a second MWPC by a distance large enough to range out betas up to 200 keV in energy.

The most challenging aspect of the low-background gaseous time-projection chamber is the construction of each radiopure MWPC. The MWPCs must be constructed from affordable materials with good radiopurity to reduce the amount of intrinsic backgrounds. They must be precision machinable to allow uniform wire gain, produce sufficiently low outgassing that electron collection is high and stable with time, and allow connections that produce sufficiently small noise that low thresholds may be achieved. This article documents the design, construction, and performance of a prototype MWPC for use in the planned ultra-low-background screener, the BetaCage. Detailed simulations of expected backgrounds in the planned screener, incorporating the MWPC design described here, are summarized in [6] and will be fully described in a separate publication [7].

2. MWPC design and construction

Each MWPC consists of two cathode grids sandwiching a crossed anode grid. The prototype MWPC is a 3-cm thick by 3.8-cm wide frame enclosing a $40.1\times40.1\,\mathrm{cm}^2$ active area, while the MWPCs for the proposed screener will have 3-cm thick by 8.3-cm wide frames that each enclose an active area of $76.7\times76.7\,\mathrm{cm}^2$; the screener's MWPC frames require additional width to help compensate for the increased strain imposed by their larger wire count. The prototype uses P-10 to characterize its performance whereas the full screener will use neon-methane as neon has no long-lived radioisotopes (argon has ^{39}Ar; a beta-emitter). To test the consistency of the design with the use of radiopure construction materials, the prototype uses materials that are known to be radiopure or available in radiopure form, with one exception: the G10 printed circuit boards used for the readout wiring, for which radiopure replacements will be discussed (§2.4). Construction of the planned screener will take place in a radon-abated cleanroom [8] to ensure that radon daughters do not contaminate critical surfaces. This section details the choice of materials, the design requirements, and the design and construction of the prototype MWPC.

2.1 Design requirements

The ability to identify beta- or alpha-emitting isotopes imposes only relatively weak requirements on the detector energy resolution and hence the gain uniformity. For alphas, a 10% energy resolution is sufficient to prevent confusion between different alpha lines; other backgrounds in this energy region are expected to be negligible. This 10% energy resolution is more than sufficient to identify beta-decay spectra, since they are identified by their endpoints, which could never be measured better than 10% with small numbers of counts. The isotope ^{210}Pb additionally has internal conversion lines in the 30-46 keV range. At the (dominant) 30 keV line, the intrinsic resolution from carrier statistics is 5.7%, so improvement of the contribution due to gain nonuniformity below 10% is not especially helpful. Gain uniformity must therefore be maintained to within $\sim$10%.

The gain G of a gaseous proportional chamber is given by the Diethorn formula [9]

$$\ln G = \frac{\ln 2}{\Delta V}\frac{\lambda}{2\pi\varepsilon_0}\ln\frac{\lambda}{2\pi\varepsilon_0 a E_{\min}(\rho_0)\rho/\rho_0}, \tag{2.1}$$

where λ is the linear charge density on the wire, ε_0 is the vacuum permittivity, a is the wire radius, ρ_0 is the density of the gas at STP, ρ is the gas density, and ΔV and $E_{\min}(\rho_0)$ are empirical properties of the gas. The parameter ΔV is the average potential required to produce at least one electron-ion pair, and $E_{\min}(\rho_0)$ is the minimum electric field required.

The expected variations in Eq. 2.1 come from voltage and pressure variations, wire displacements, and wire-diameter variations [10, 11, 12]. The capacitance and potential of the anode with respect to the cathode grids sets λ. A 5% gain variation can result from a 2.5 V (0.2%) high-voltage source variation, a 1.5% wire-diameter variation, or a 100 μm (2%) anode-wire displacement (*cf.* Fig. 1). There is no avalanching at the cathode wires, so their positioning is not as important. Nevertheless, as detailed in §2.3, the prototype's cathode and anode wires were positioned to within similar tolerances.

2.2 Block-frame design

The MWPC frame is constructed from a high-density plastic called Noryl.[1] The frame was precision machined into four bars, two that hold the anode wires and two that contain the crossed

---

[1] Originally developed by GE Plastics in 1966, Noryl is a proprietary amorphous blend of polyphenylene oxide (PPO) and polystyrene (PS) that exhibits excellent hydrolytic and dimensional stability as well as good processability [13]. Screening using a variety of techniques indicates acceptable bulk contamination levels for ^{238}U, ^{232}Th and ^{40}K of $\leq$1, 3 and 5 mBq/kg, respectively [6]. While other plastics may be suitable, Noryl was attractive for these reasons as well as its low cost. Acrylic, for example, is not as easily machined.

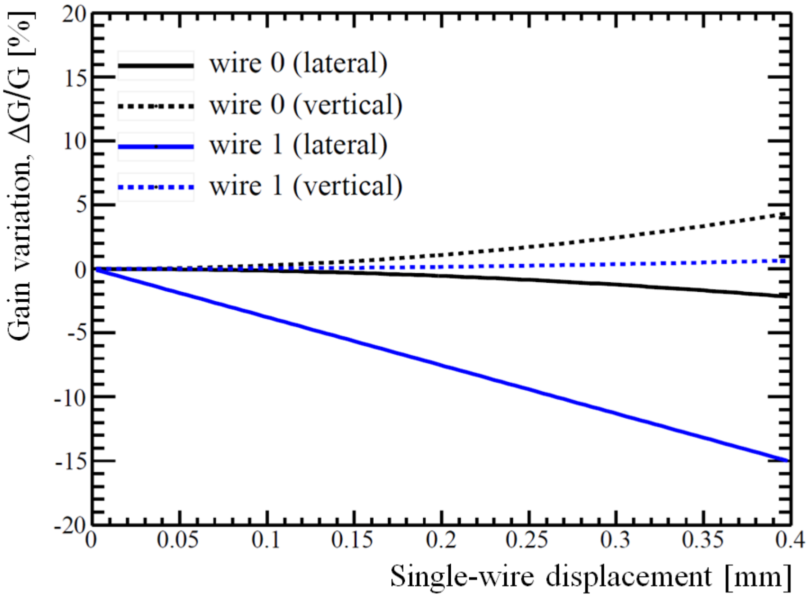

Figure 1. Expected gain variations due to a single wire displacement, both on the displaced wire (wire 0, upper dotted and solid curves) and its nearest neighbor (wire 1, lower dotted and solid curves), where vertical and lateral displacements correspond to deviations out of and in the plane of the MWPC, respectively.

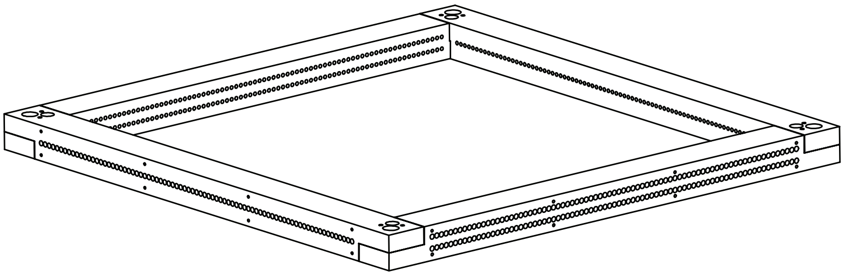

Figure 2. Mechanical drawing of the Noryl block-frame design for the prototype MWPC. The 3-cm thick by 3.8-cm wide frame encloses a $40.1 \times 40.1\,\mathrm{cm}^2$ active area. The anode and cathode layers are defined by the two sides with a single and double row of holes, respectively. There are 79 wires per layer positioned by press-fit, spring-loaded feedthroughs to give a 5 mm inter-wire and -layer pitch.

cathode layers. Figure 2 shows a mechanical drawing of the prototype frame. Each layer contains 79 wires with a pitch of 5 mm. The anode-wire plane is also 5 mm from each cathode-wire plane. The four frame pieces were rough-cut, annealed, and finish-cut to a 20 μm (or better) flatness, and then holes for the spring-loaded feedthroughs that hold the wires were drilled. The feedthroughs have a tapered shoulder in the middle for seating. The four pieces were arranged as shown in Fig. 2 with stainless-steel alignment pins and bolted together. A 0.5 inch through-hole was drilled into each corner to facilitate connection to either a stand or fieldcage. For the prototype frame, these holes were additionally used to bolt on copper-clad G10 sheets, the purpose of which is discussed in §3.2.

2.3 Spring-loaded feedthroughs

To prevent gravitational sag, the wires are maintained at uniform tension through the use of custom-design feedthroughs. Each wire is held in place at one end by a spring-loaded feedthrough consisting of two precision-machined brass pieces, a spring, and an annealed copper tube (*cf.* lower drawing in Fig. 3a). At the other end, the wire is held by a simpler, spring-less feedthrough consisting of a single brass piece and an annealed copper tube (*cf.* upper drawing in Fig. 3a). The wires are first threaded through the spring-side feedthrough and anchored by crimping its copper tube. The anode (cathode) wires are then threaded through the opposing, spring-less feedthrough, tensioned at 20 g (200 g) using a weight and pulley, and finally secured by crimping the second copper tube. In addition to gripping the wires, the crimps establish electrical connections between the wires and copper tubes, which are used to instrument signal readout and provide high voltage.

As discussed in §2.1, to prevent significant gain variations due to misplacement, a 100 μm tolerance was specified for the positioning of each wire. To achieve this, the feedthroughs were designed to be press-fit into the MWPC frame with a precision in position better than 25.4 μm. Further, each press-fit brass piece was designed with an anode (cathode) wire hole with a diameter of 101.6 μm (177.8 μm) centered to better than 25.4 μm, thereby accurately guiding each 25.4-μm (127-μm) diameter stainless-steel anode (cathode) wire.[2] Following fabrication, the prototype MWPC frame and press-fit brass pieces were surveyed, indicating realized tolerances of 20 and 10 μm, respectively. The resulting displacement is thus expected to be $<$45 μm, well within the design specification described in §2.1 to maintain uniform gain.

All of the above elements (stainless-steel wire, brass pieces, copper tubes, springs) can be readily made from radiopure stock. Further, the wire can be electropolished to remove surface radiocontaminants such as ^{210}Pb and ^{210}Po [15, 16].

2.4 Wire stringing

The MWPC wires were strung by hand using a multi-step procedure (see also appendix C in [17]). As demonstrated in Fig. 4a, each wire was guided through opposing feedthrough holes using a long aluminum rod inserted through the holes to pull the wire back through the frame. The end of the wire at the spring-side was then threaded through the fully assembled spring-side feedthrough with the help of suction on the end of its copper tube (via a weak vacuum). With the threaded feedthrough held in place by a custom jig containing a pneumatic crimp tool, the feedthrough's copper tube was crimped, and the whole feedthrough was carefully press fit into the frame. The opposite end of the wire was then inserted into the spring-less feedthrough, also with the help of suction. Before tensioning the wire, the feedthrough was carefully press fit into the frame and a similar crimping jig was moved into place. A custom-machined aluminum bar with the same hole pattern as the frame was affixed to a nearly frictionless slide. A weight, hanging from the bar using a low-friction pulley, provided tension to the wire, at which point the spring-less feedthrough's

---

[2] Gauge 50 (36) type 304 stainless-steel wire from the California Fine Wire Co. was used for the anode (cathode) [14].

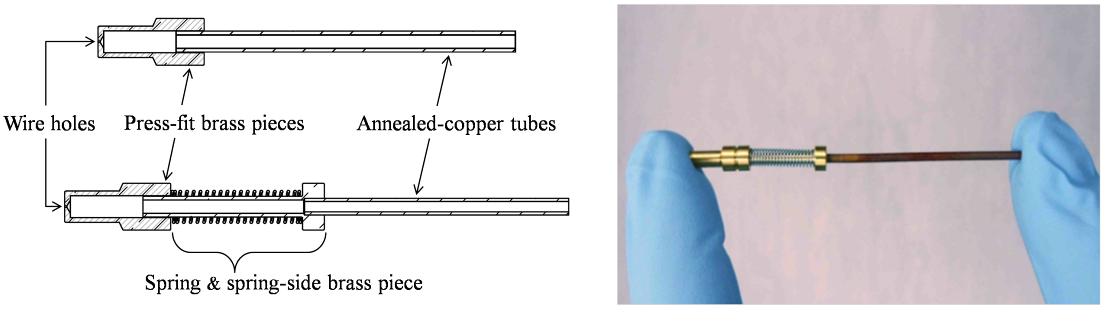

a) b)

Figure 3. a) Mechanical drawings of the two feedthroughs used to position and tension each wire. Stringing starts by threading the spring-side feedthrough (lower drawing) with a stainless-steel wire and crimping the copper tube (to hold the wire in place). The feedthrough is then press fit into one side of the MWPC frame, and the wire is strung across the frame to the opposing side and threaded through a simpler, spring-less feedthrough (upper drawing), where it is tensioned and finally secured by crimping the second copper tube. b) Photograph of a spring-side feedthrough.

copper tube was crimped. It took 6 minutes to string a single wire. The fully strung prototype MWPC is shown in Fig. 4b.

The final step in the MWPC assembly was to affix custom printed circuit boards (PCBs) to two edges of the frame. Fly-wires crimped to the ends of the copper tubes were then attached to the PCBs, thereby establishing electrical connections from the MWPC wires to coaxial cabling (soldered directly to pads on the PCBs). The coaxial cabling used is Ag-coated Cu with Kapton insulation (Accu-Glass Products model TYP32-15 [18]). Cabling of similar construction has been measured to be radiopure [19]. This final step will be different for the planned screener: the G10-based PCBs used in the prototype will be replaced with (more expensive) Cirlex,[3] a material widely used in dark matter experiments because of its radiopurity [21], low outgassing rate, and well-known mechanical properties (see *e.g.* [22]), and low-radioactivity solder [23] will be used.

Radon daughter contamination of the wires during stringing will be prevented by undertaking construction in a radon-abated cleanroom [8].

3. Prototype MWPC test setup

In this section, the experimental configuration used to test the energy response and operational stability of the prototype MWPC is reviewed. The completed frame was placed inside a stainless-steel pressure vessel that was connected to a rudimentary gas-handling system, providing a controlled space for the introduction of a drift gas. Electrical connections were made via SHV vacuum feedthroughs attached to the bottom of the vessel, enabling application of an electric field and signal readout.

3.1 Gas handling

Ultimately, the planned screener will be operated with a neon-methane mixture. Neon is preferred

---

[3] Cirlex is an adhesiveless sheet material made from DuPont's Kapton polyimide and offered by Fralock [20].

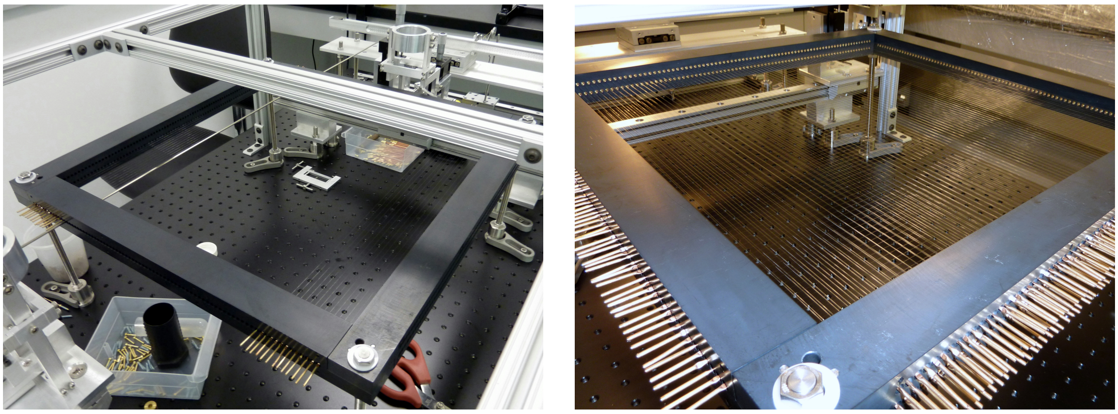

a)　b)

Figure 4. a) Photograph of the setup used to string the prototype MWPC frame. During the stringing process, the frame was secured to an optical table via threaded rods at each of the four corners and surrounded by a T-slotted aluminum frame to help protect the wires. Custom-design fixtures for positioning a crimping tool were located on rails just outside opposing sides of the anode frame pieces. An aluminum rod was used to unspool wire from the far side and through two opposing frame holes. After anchoring the wire to the frame via the spring-side feedthrough (near side), it was tensioned using an aluminum bar attached to a low-friction slide (top of photo behind crimping fixture) and secured via the spring-less feedthrough. The frame was rotated 90° in order to string the cathode layers. b) Photograph of the fully-strung MWPC prototype. Assembly was completed by crimping fly-wires to the copper tubes along the outer edges of two adjacent sides of the frame. The fly-wires were connected to custom circuit boards mounted directly to the frame.

because it has no naturally-occurring long-lived radiocontaminants, making it an ideal medium for low-background screening. Additionally, its stopping power is low enough that the trigger MWPC can be thick enough (1 cm) to make assembly straightforward. For tests with the prototype, the more common (and less expensive) P-10 gas—a mixture of 90% Ar and 10% CH_4—was chosen for the detection medium. The average energy loss of an incident particle to create a single electron-ion pair in this mixture is $W = 26\,\mathrm{eV}$ [24]. Therefore, 38.5 ± 2.6 electron-ion pairs are created per keV of deposited energy.[4]

The gas-handling system consisted of a gas cylinder, an input manifold, and a turbo and roughing pump. The pressure vessel was first pumped down to a vacuum between 10^{-3}–10^{-5} Torr before filling with room-temperature P-10 gas (purchased premixed). The P-10 mixture was allowed to flow freely into the chamber and was monitored with an analog relative-pressure gauge. Flow was terminated (by hand) once a slight overpressure of 0.5 psig was achieved, thus minimizing contamination of the detection gas due to laboratory air leaking into the pressure vessel. Since the gas gain varies only linearly with pressure, this somewhat crude introduction of P-10 gas was sufficient to characterize the MWPC response; as shown in Fig. 8, the gain varied by (at most) a few percent due to the resulting pressure variation. Eventually, an MKS 902 piezoelectric transducer [25] was added to monitor pressure to an accuracy of 1%, permitting the measurements discussed in §4.2.

The gas-handling system for the planned screener will include measures to avoid radon con-

---

[4] The Fano factor in P-10 gas is 0.17 [24].

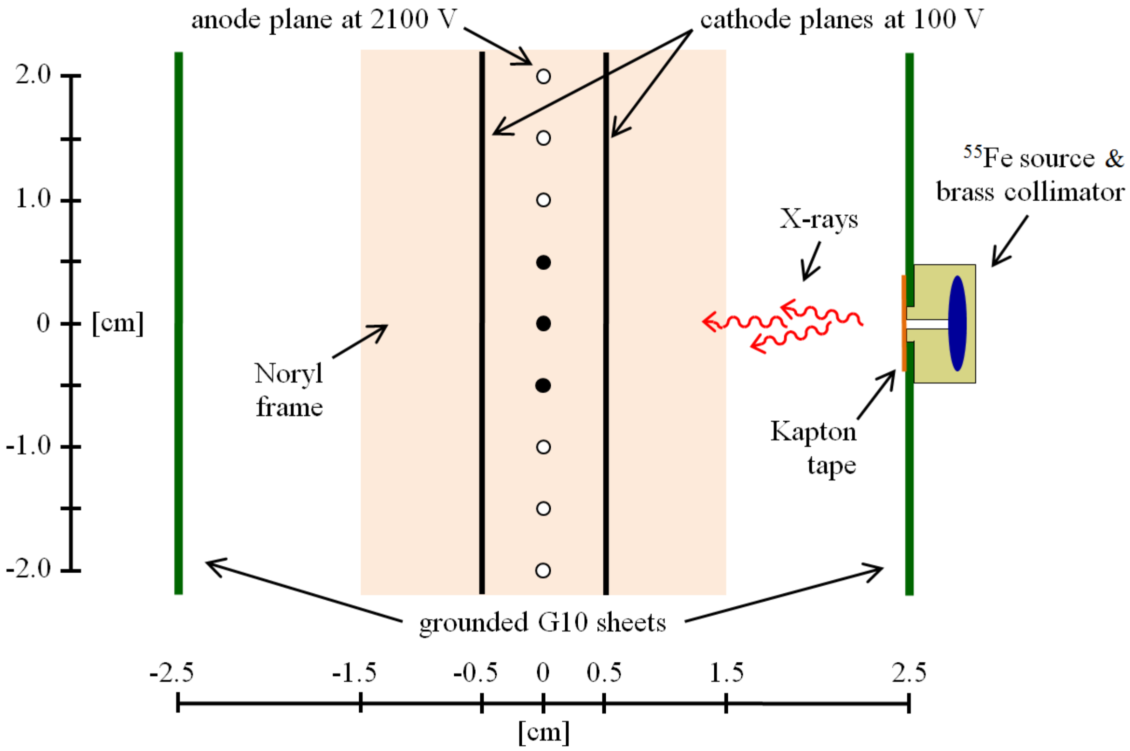

Figure 5. Diagram of the drift-field and ^{55}Fe-source configuration used to test the prototype MWPC, highlighting the center of its crossed wire planes and drawn to scale. The three central anode wires (dark dots) were read out as a single channel, while the others (light dots) were biased but otherwise uninstrumented. The shaded region corresponds to the Noryl frame's 3 cm thickness. Except for the Fig. 6 spectrum, all tests were made with the copper-clad G10 sheets attached to the Noryl frame via 1-cm thick nylon spacers, yielding a 2 cm drift region for ionization electrons created between the Kapton tape and right-side cathode wires (as shown). The data featured in Fig. 6 were obtained with an earlier configuration in which the G10 sheets were bolted to the frame without spacers, resulting in a 1 cm drift region. This difference should have little to no effect on the energy response.

tamination [6], reducing deposition of radon daughters in the screener (especially on the MWPC wires), but such measures were not taken for the tests reported here.

3.2 Readout electronics

A simple single-channel data acquisition (DAQ) was used to test the performance of the MWPC. The three central anode wires were ganged together (on the PCBs described in §2.4) and read out as a single channel. The remaining anode wires were held at the same potential—ranging from 1900–2250 V for most tests—but were otherwise uninstrumented. During standard operations, the anode was biased to 2100 V, while the cathode planes were kept at a small, 100 V potential to create a 2 cm drift region between the cathode and the grounded G10 sheets bolted to the MWPC frame (as indicated in Fig. 5).

The anode and cathode potentials were maintained by a Bertan Model 375P high-voltage power supply [26], designed specifically for MWPC operation. Since the gas gain is proportional to

(λ^{λ}), the voltage source must be extremely stable to prevent significant gain variations. The high voltage was additionally conditioned by a two-stage low-pass filter with a 72 Hz cut-off frequency. All MWPC wires were biased with one end floating.

A Cremat CR-111 [27] two-stage charge amplifier was used to shape and amplify signals from the central three anode wires. Its first stage is a high-gain integrating amplifier with feedback resistance $R_{\mathrm{f}} = 10\,\mathrm{M}\Omega$ and feedback capacitance $C_{\mathrm{f}} = 15\,\mathrm{pF}$, yielding a $150\,\mu\mathrm{s}$ output-pulse decay time. The second stage is a low-gain amplifier intended to drive an output signal through a coaxial transmission line. The rise time at the CR-111 output (3 ns according to the manufacturer) is found to be faster than the digitization rate even with the additional input capacitance of the MWPC and so has no impact on the analyses. Similarly, the CR-111 gain (0.13 V/pC according to the manufacturer) has not been verified experimentally, as its precise value is not critical; it is used only for confirmation of the Diethorn relation (§4.2 and Fig. 9).

A National Instruments PCI-5105 ADC [28] was used to digitize the CR-111 output with 12-bit resolution at a rate of 250 kS/s. The PCI-5105 was operated in continuous read digitization mode.[5] One-second-long traces were acquired starting at random times, and pulses were identified by searching for peaks in the time derivative of the traces. Pulse heights were estimated from the peak values in the undifferentiated time stream of the identified pulses. To reduce high-frequency noise, a 6th-order Butterworth filter with a 10 kHz cut-off frequency was applied to the raw traces prior to these steps. This technique was used to measure pulse-height spectra, study pulse pile-up, and to estimate absolute rates.

Electronic noise was estimated from pulse-free sections of the same one-second-long, digitally filtered traces, yielding $\sim$2 mV FWHM. This corresponds to $\sim 10^5$ electrons FWHM at the CR-111 input, substantially poorer than the 1500–2500 electrons FWHM expected for the CR-111 from the manufacturer specifications and allowing an input capacitance range of 0–120 pF. As discussed in §4.1, even this high noise is subdominant compared to Fano and avalanche statistics and thus does not impede a demonstration that the MWPC provides near statistics-limited energy resolution, which was the goal of this effort.

4. MWPC performance

To assess the performance of the prototype MWPC, several tests were conducted using x-rays from an ^{55}Fe source. Energy resolution and gain were measured as functions of voltage, pressure, and time, and estimates of the Diethorn parameters ΔV and E_{min} were extracted.

4.1 Energy resolution and gain

^{55}Fe decays via electron capture with a half-life of 2.73 years, producing Mn K-shell x-rays at 5.89 and 6.49 keV. The 5.89 keV x-rays have almost an order of magnitude larger branching fraction than the 6.49 keV x-rays. Further, in gaseous detectors the two energies tend to be indistinguishable due to the relatively large statistics-limited energy resolution. The source activity at the time of the measurements was $26.5\,\mu$Ci. Its active region is $\sim$3 mm in diameter. The choice of argon as the detection gas also introduces a 2.9 keV escape peak to the spectrum. When an x-ray ionizes a

---

[5] The PCI-5105 offers a triggered mode, but the software-limited live time was unacceptable.

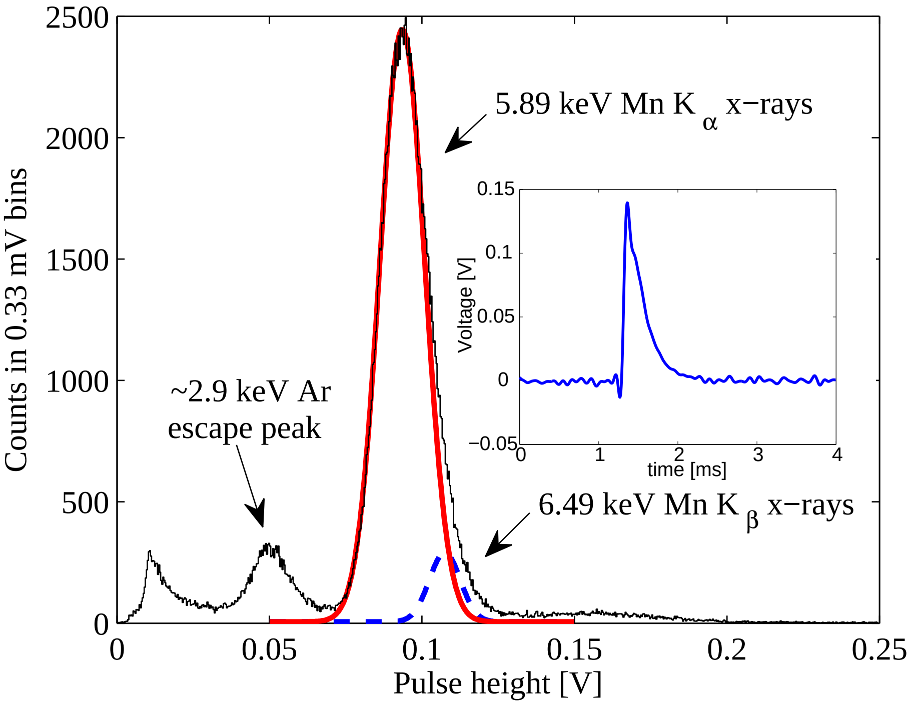

Figure 6. Pulse-height spectrum recorded with the prototype MWPC when exposed to an ^{55}Fe source at anode and cathode potentials set to 2100 and 100 V, respectively. The Mn K-shell x-rays are observed as a single peak with the addition of an $\sim$2.9 keV Ar escape peak. The sources of the 0.01 V peak and the broad hump in the 0.13–0.20 V region are not known with certainty, but they have no impact on the K-shell peak fits. A combination of two Gaussians and a linear background was fit to the region with pulse heights $\gtrsim$0.07 V, where the means of the two Gaussians were constrained to have the expected 6.49-to-5.89 ratio. This hypothesis has a χ^2/d.o.f. = 502/487 and yields a FWHM resolution of 15.8% for the 5.89 keV peak, close to the minimum possible value of 12–13% (*cf.* §4.1 and appendix A). The best-fit Gaussians for the 5.89 keV (solid) and 6.49 keV (dashed) peaks are shown independently without the linear background. Inset: A typical $\sim$6 keV pulse taken under the same conditions following application of a digital low-pass filter.

K-shell electron in Ar, the Ar atom emits an Ar K-shell x-ray with an energy of 3 keV due to the filling of the K-shell vacancy. This 3 keV x-ray has a longer absorption length than a higher-energy x-ray and so may escape the detection region, resulting in a peak 3 keV below that of the primary x-ray. This is actually a collection of lines, making it difficult to fit for the energy resolution.

The ^{55}Fe source was centered on the MWPC immediately outside the drift region external to the copper-clad G10 ground plane (*cf.* Fig. 5). The source was affixed to a 3.2-mm thick gold-plated copper collimator with a 1-mm diameter circular aperture. The front of the collimator was covered with a thin layer of Kapton tape to prevent electrons created outside the drift region from entering it. Note that the source and G10 sheet would not be installed during low-background operation of the planned screener.

To search for the 5.89 keV x-rays, a voltage scan was performed near an anode potential of 2100 V. These scans were taken both with and without the source present to confirm that any spec-

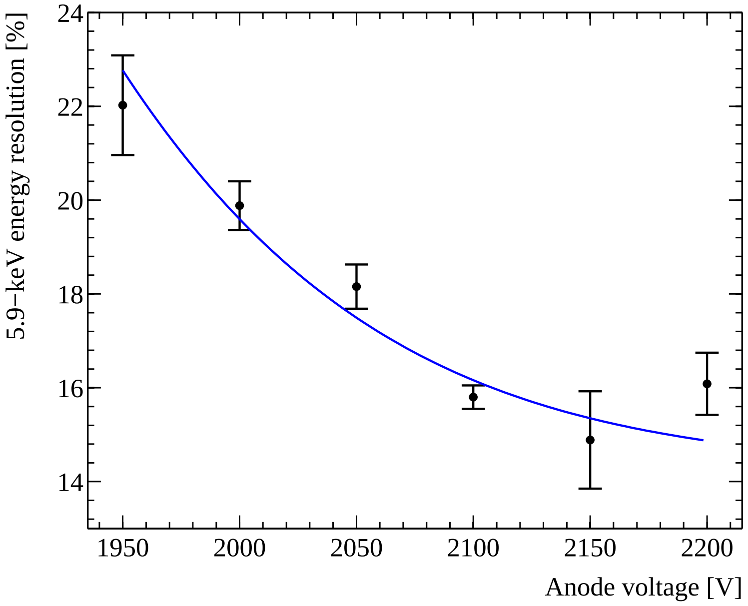

Figure 7. Measured FWHM energy resolution of the 5.89 keV peak as a function of voltage. The resolution degrades with decreasing bias voltage due to an increasing contribution from a gain-dependent term in the relative resolution function (*cf.* Eq. 4.1). The data (dots with 1σ error bars) were taken in 1-minute intervals except at 2100 V, for which a 20-minute acquisition was performed. The best-fit estimate (χ^2/d.o.f. $= 8.5/4$) for the FWHM intrinsic resolution from Fano and avalanche statistics is $14.2 \pm 0.8\%$.

tral features could indeed be attributed to the ^{55}Fe source. Once the peak was located, the voltage was tuned to bring the x-ray and escape peaks well above the noise threshold. Figure 6 shows the pulse-height spectrum of an ^{55}Fe-source run taken with anode and cathode potentials of 2100 and 100 V, respectively. The Mn K-shell x-rays are observed along with an $\sim$2.9 keV escape peak. The best-fit mean of the 5.89 keV peak was used to calibrate the energy scale and yields a gain of $\sim 10^4$.

The 5.89 keV peak fit featured in Fig. 6 yields a FWHM energy resolution of 15.8%. Figure 7 demonstrates that the resolution improves with increasing gas gain (anode voltage) in the manner one would expect for the quadrature sum of a term due to Fano and avalanche statistics, FWHM_0, and a term, $\mathrm{FWHM}_{\mathrm{other}}$, whose contribution decreases with increasing gas gain (due to, *e.g.*, electronic noise):

$$\mathrm{FWHM} = \sqrt{\mathrm{FWHM}_0^2 + \frac{\mathrm{FWHM}_{\mathrm{other}}^2}{\bar{G}^2}}, \tag{4.1}$$

where $\bar{G}$ is the pulse-height gain as a function of anode voltage normalized to the gain at 2100 V. The values obtained at 5.89 keV are $\mathrm{FWHM}_0 = 14.2 \pm 0.8\%$ and $\mathrm{FWHM}_{\mathrm{other}} = 7.6 \pm 1.0\%$. As discussed in appendix A, the former is close to the minimum resolution of 12–13% from Fano and avalanche statistics expected for our chamber configuration at 5.89 keV. The good agreement of the measurement with this value suggests that any non-statistical contribution to FWHM_0 is smaller than the measurement precision. The electronic-noise contribution is $\mathrm{FWHM}_{\mathrm{elec}} \approx 2.2\%$ based on the electronic noise of $\sim$2 mV FWHM from §3.2 and the observed 5.89 keV pulse height of 90 mV, and thus $\mathrm{FWHM}_{\mathrm{other}}$ is appreciably larger than expected from electronic noise alone. However,

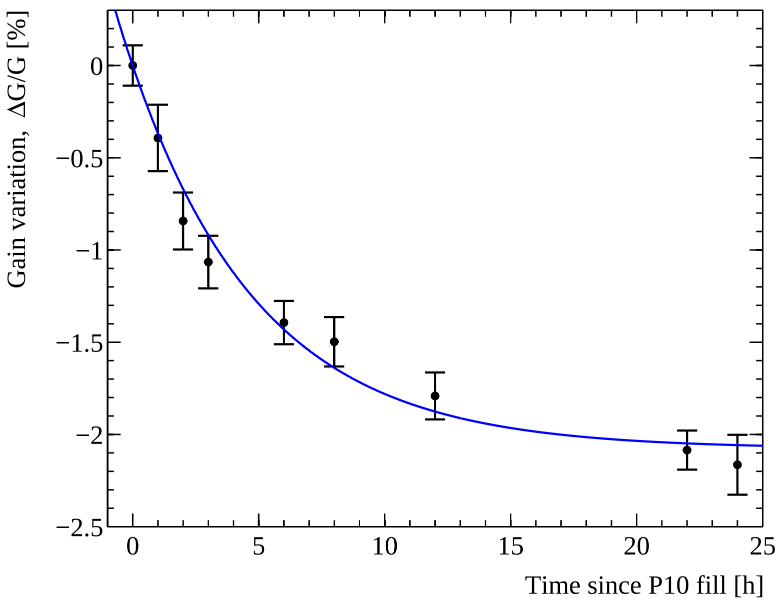

Figure 8. Stability of the gain (*vs.* time) following a P-10 gas fill. A series of ^{55}Fe-source runs were taken over the course of a day, with the means of the resulting 5.89 keV peaks indicating a slight, few-percent degradation in gain (dots with 1σ error bars). Attributed to drift-gas contamination due to outgassing from detector materials, the degradation is well-fit by a two-parameter exponential form (*cf.* Eq. 4.2) with a χ^2/d.o.f. = 4.6/7, an amplitude $A_{\text{stability}} = -2.08 \pm 0.09\%$, and a $1/e$ decay time $\tau_{\text{stability}} = 5.1 \pm 0.7$ h.

during typical operation for beta screening, the energy per 5-mm cell will be approximately 1 keV, at which energy the theoretical statistics-limited resolution will scale by $1/\sqrt{E}$ to approximately 30% FWHM, likely rendering any such non-statistical contribution, as well as the electronic noise, negligible. Furthermore, any such non-statistical and electronic noises will decrease with upgrades to the electronics, gas-handling system, and a position-corrected analysis.

4.2 Detector characterization

To assess the prototype's operational stability, several short ^{55}Fe-source runs were recorded over the course of a day subsequent to a P-10 gas fill. Figure 8 shows the resulting stability of the gain, measured by the location of the 5.89 keV peak, as a function of time. The observed gain variation is well-fit by an exponential trend:

$$\frac{\Delta G}{G} = A_{\text{stability}} \left(1 - e^{-t/\tau_{\text{stability}}}\right), \tag{4.2}$$

where t is time since the P-10 gas fill. The best-fit amplitude $A_{\text{stability}} = -2.08 \pm 0.09\%$, and the best-fit decay constant $\tau_{\text{stability}} = 5.1 \pm 0.7$ h. The primary reason for the gain drift is attributed to outgassing from the various detector components. For the planned screener, the detection gas will be continuously circulated through a SAES MC190-902F MicroTorr purifier [29] and a (custom-design) cooled-carbon radon trap [6] to help remove outgassed contaminants and thus further improve gain stability.

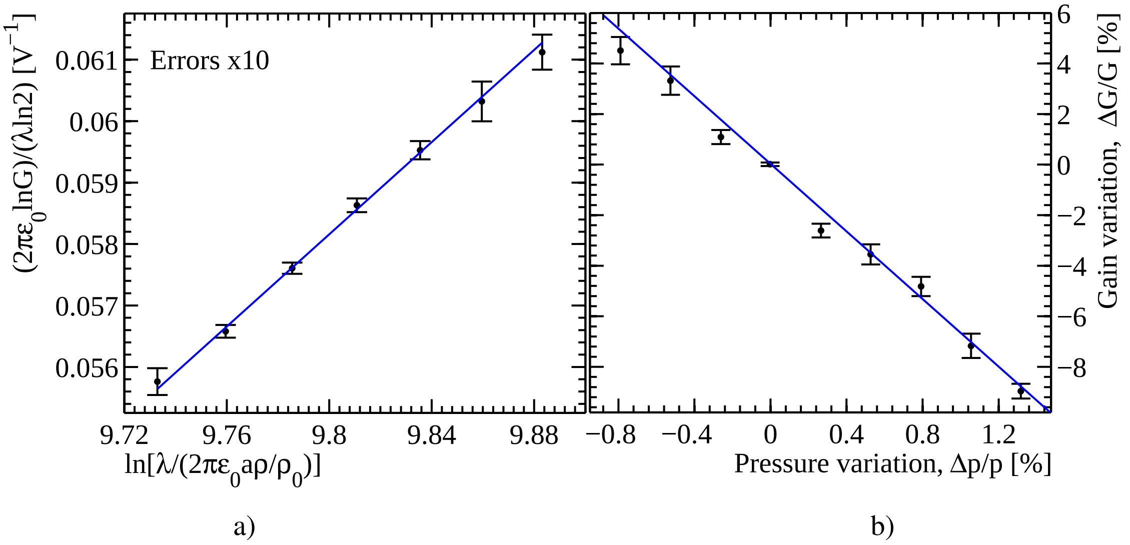

Figure 9. a) Test of the Diethorn formula for gas gain in a proportional chamber, where Eq. 2.1 has been rearranged to yield a linear relationship with varying anode voltage (dots with exaggerated 1σ error bars). An estimate of the Diethorn parameters is extracted with a linear fit; $\Delta V = 26.7 \pm 0.6$ V and $E_{\text{min}} = 38.3 \pm 1.3$ kV/cm, in agreement with expectation. b) Gain variation, as measured with 5.89 keV x-rays, as a function of pressure change (dots with 1σ error bars). The Diethorn formula predicts a slope of -6.5 ± 0.3 that is confirmed by a best-fit slope of -6.7 ± 0.3.

The Diethorn parameters ΔV and E_{min} were estimated with a fit to $(2\pi\varepsilon_0 \ln G)/(\lambda \ln 2)$ as a function of $\ln|\lambda/(2\pi\varepsilon_0 a\rho/\rho_0)|$ (*cf.* Fig. 9a), where the variation in the charge density results from varying the high voltage. This linear relationship allows for easy extraction of the Diethorn parameters; $\Delta V = 26.7 \pm 0.6$ V and $E_{\text{min}} = 38.3 \pm 1.3$ kV/cm,[6] with expectations of 23.6 ± 5.4 V and 48 ± 3 kV/cm, respectively [30].[7] All uncertainties are statistical at 1σ confidence.

An additional check on the performance of the MWPC is to vary the pressure and monitor the corresponding change in gain. Figure 9b shows this measurement, again using the location of the 5.89 keV peak to track the gain. This linear relationship between gain and pressure is expected to have a slope of -6.5 ± 0.3 [10]. The best-fit slope to the data in Fig. 9b is -6.7 ± 0.3.

Table 1 compares the expected values of several characteristic MWPC parameters to those measured with the prototype. Where appropriate, all parameters match to within statistical uncertainties, with E_{min} to within the spread of previous measurements [10]. The spread is most likely due to slight impurities in the detection gas. As dependence of the gain on this parameter is somewhat muted due to a logarithm, the modest inconsistency with previous values is not a concern.

5. Conclusion

A prototype low-background MWPC for the detection of alphas and low-energy betas has been constructed and characterized. This device performs well down to a few keV in deposited energy

---

[6] Assuming the nominal 0.13 V/pC gain of the Cremat CR-111 amplifier [27].

[7] Historically, there is a wide range of measured E_{min} values that encompass this estimate [10].

Table 1. Comparison of several expected gas parameters with those measured with the prototype MWPC. As outgassing is hard to predict, there is no expectation for the two stability parameters. All uncertainties are quoted at 1σ confidence.

parameter	description	expected	measured	units
FWHM_0	intrinsic resolution @ 5.89 keV	12–13	14.2 ± 0.8	%
$A_{\mathrm{stability}}$	gain-stability amplitude		-2.08 ± 0.09	%
$\tau_{\mathrm{stability}}$	gain-stability $1/e$ decay time		5.1 ± 0.7	h
E_{min}	Diethorn minimum electric field	48 ± 3	38.3 ± 1.3	kV/cm
ΔV	Diethorn electron-ion potential	23.6 ± 5.4	26.7 ± 0.6	V
$\frac{\partial(\Delta G/G)}{\partial(\Delta p/p)}$	gain *vs.* pressure slope	-6.5 ± 0.3	-6.7 ± 0.3	

as shown by the measurement of x-rays produced from ^{55}Fe decays. The MWPC was found to respond with an energy resolution of 15.8% at 5.89 keV and a gas gain of $\sim 10^4$, close to the expected statistical limit. Further improvements to this resolution will come from planned electronics upgrades to include position information. The gain is stable to $\sim$2% for $>$1-day periods and is expected to have negligible instability with a planned upgrade to the gas-handling system that includes a continuous circulation loop with gas purification. Further, gain variations due to pressure changes fall in line with expectation and can be corrected with accurate pressure monitoring. This prototype MWPC has met or exceeded all of its design goals.

Acknowledgments

This work was supported in part by the National Science Foundation (Grants No. PHY-0834453 and PHY-0855525), the Department of Energy HEP division, and the University of Alberta Department of Physics and Faculty of Science. The authors gratefully acknowledge the technical contributions of L. Buda, J. Hanson, G. Lachat, and P. Zimmerman, and the quality-control testing of J. Roberts and M. Mintskovsky.

A. Intrinsic Energy Resolution

Intrinsic proportional-chamber resolution at energy E can be estimated using Eq. 6.24 in [31]:

$$\mathrm{FWHM}_0 = 2.35\sqrt{\frac{W(F+b)}{E}}, \tag{A.1}$$

where $W = 26\,\mathrm{eV}$ is the average energy required to form one electron-ion pair in P-10 [24], $F = 0.17$ is the Fano factor for P-10 [24], and b is the avalanche factor and depends not only on the gas type but also on the chamber's pressure and anode-wire radius. We estimate $b \approx 0.44$ following Alkhazov's model [32], as summarized in [31, 33, 34]. Alkhazov's model appears to agree well with experimental data for argon-methane chambers with gas gains between $\sim$100 and 10^5 (see, *e.g.*, [35]). We start with $b = 0.5$, calculated using Alkhazov's model for a gas gain of 100 and a pressure×anode-radius product of 0.5 Torr-cm [33]. Using the figures in [34] (also from

Alkhazov's model), we scale down by 18% to account for our chamber's smaller pressure×anode-radius product ($\sim$0.01 Torr-cm) and then up by 7.5% to account for the larger gas gain ($\sim 10^4$), yielding $b \approx 0.44$ and a minimum FWHM$_0$ at 5.89 keV of $\sim$12%.

Of course, Alkhazov's model has not been fully verified as it is impossible to construct a perfect chamber. The measurement in [33] of 13.2% at 5.89 keV is the lowest resolution using P-10 in the literature and is very close to the model's predicted 12.8%. Treating this measurement as an upper limit on the resolution due to Fano and avalanche statistics implies $b \leq 0.55$ for the device used in [33], which, if scaled with pressure×anode-radius product and gas gain to our chamber's parameters as was done above, suggests $b \lesssim 0.5$. To encompass this experimental uncertainty, a minimum expected FWHM$_0$ of 12–13% is used in this paper, corresponding to $b = 0.44$–0.5.

References

[1] J. A. Formaggio and C. J. Martoff, *Backgrounds to sensitive experiments underground*, *Ann. Rev. Nucl. Part. Sci.* **54** (2004) 361–412. doi:10.1146/annurev.nucl.54.070103.181248.

[2] R. W. Schnee, Z. Ahmed, S. R. Golwala, D. R. Grant, and K. Poinar, *Screening Surface Contamination with BetaCage*, in *Topical Workshop on Low Radioactivity Techniques: LRT 2006*, vol. 897, pp. 20–25, AIP Conf. Proc., Mar. 28, 2007. doi:10.1063/1.2722063.

[3] G. Charpak *et al.*, *The use of multiwire proportional counters to select and localize charged particles*, *Nucl. Instrum. Meth.* **62** (1968) 262–268. doi:10.1016/0029-554X(68)90371-6.

[4] T. Shutt, C. E. Dahl, L. DeViveiros, R. J. Gaitskell, and R. W. Schnee, *Beta Cage: A New, Large-Area Multi-Wire Screening Detector For Surface Beta Contamination*, in *Topical Workshop on Low Radioactivity Techniques: LRT 2004*, vol. 785, pp. 79–83, AIP Conf. Proc., Sep. 8, 2005. doi:10.1063/1.2060456.

[5] Z. Ahmed, S. R. Golwala, D. R. Grant, M. Kos, R. H. Nelson, R. W. Schnee, and B. Wang, *Status of BetaCage: an Ultra-sensitive Screener for Surface Contamination*, in *Topical Workshop on Low Radioactivity Techniques: LRT 2010* (R. Ford, ed.), vol. 1338, pp. 88–92, AIP Conf. Proc., Apr. 27, 2011. doi:10.1063/1.3590914.

[6] R. Bunker, Z. Ahmed, M. A. Bowles, S. R. Golwala, D. R. Grant, M. Kos, R. H. Nelson, R. W. Schnee, A. Rider, B. Wang, and A. Zahn, *The BetaCage, an ultra-sensitive screener for surface contamination*, in *Topical Workshop on Low Radioactivity Techniques: LRT 2013* (L. Miramonti and L. Pandola, eds.), vol. 1549, pp. 132–135, AIP Conf. Proc., Apr., 2013. doi:10.1063/1.4818093.

[7] Z. Ahmed, M. A. Bowles, R. Bunker, S. R. Golwala, D. R. Grant, M. Kos, R. H. Nelson, R. W. Schnee, and B. Wang, "Expected Background for the BetaCage." *Paper in preparation*.

[8] R. W. Schnee, R. Bunker, G. Ghulam, D. Jardin, M. Kos, and A. S. Tenney, *Construction and measurements of a vacuum-swing-adsorption radon-mitigation system*, in *Topical Workshop on Low Radioactivity Techniques: LRT 2013* (L. Miramonti and L. Pandola, eds.), vol. 1549, pp. 116–119, AIP Conf. Proc., Apr., 2013. doi:10.1063/1.4818089.

[9] W. Diethorn, *A methane proportional counter system for natural radiocarbon measurements*, Report NY06628, USAEC, 1956.

[10] W. Blum, W. Riegler, and L. Rolandi, *Particle Detection with Drift Chambers*. Springer, second ed., 2008.

[11] F. Sauli, “Principles of Operation of Multiwire Proportional and Drift Chambers.” CERN-77-09, 1977. Lectures given in the Academic Training Programme of CERN 1975–1976.

[12] G. A. Erskine, *Electrostatic problems in multiwire proportional chambers*, *Nucl. Instrum. Meth.* **105** (1972) 565–572. doi:10.1016/0029-554X(72)90356-4.

[13] SABIC Innovative Plastics, Pittsfield, MA 01201, USA. www.sabic-ip.com.

[14] California Fine Wire Co., Grover Beach, CA 93483, USA. www.calfinewire.com.

[15] R. W. Schnee, M. A. Bowles, R. Bunker, K. McCabe, J. White, P. Cushman, M. Pepin, and V. E. Guiseppe, *Removal of long-lived* ^{222}*Rn daughters by electropolishing thin layers of stainless steel*, in *Topical Workshop on Low Radioactivity Techniques: LRT 2013* (L. Miramonti and L. Pandola, eds.), vol. 1549, pp. 128–131, AIP Conf. Proc., Apr., 2013. doi:10.1063/1.4818092.

[16] G. Zuzel and M. Wójcik, *Removal of long-lived* ^{222}*Rn daughters from copper and stainless steel surfaces*, *Nucl. Instrum. Meth. A* **676** (2012) 140–148. doi:10.1016/j.nima.2011.12.043.

[17] Z. Ahmed. PhD thesis, California Institute of Technology, 2012. cdms.berkeley.edu/Dissertations/ahmed.pdf.

[18] Accu-Glass Products, Inc., Valencia, CA 91355, USA. accuglassproducts.com.

[19] E. Aprile *et al.*, *Material screening and selection for XENON100*, *Astropart. Phys.* **35** (2011) 43–49. doi:10.1016/j.astropartphys.2011.06.001.

[20] Fralock Div. Lockwood Ind., Canoga Park, CA 91304, USA. www.fralock.com.

[21] J. Loach, J. Cooley, A. Cox, A. Poon, K. Adler, M. Bruemmer, K. Nguyen, and B. Wise, *A material assay database for the low-background physics community*, in *Topical Workshop on Low Radioactivity Techniques: LRT 2013* (L. Miramonti and L. Pandola, eds.), vol. 1549, pp. 8–11, AIP Conf. Proc., Apr., 2013. doi:10.1063/1.4818064.

[22] R. Alon *et al.*, *Operation of a thick gas electron multiplier (THGEM) in Ar, Xe and Ar-Xe*, *JINST* **3** (2008) P01005. doi:10.1088/1748-0221/3/01/P01005.

[23] D. S. Akerib, A. da Silva, D. L. Hurley, B. Pritychenko, B. Sadoulet, and A. Smith, *Production of solder and flux with low radioactivity*, *Nucl. Instrum. Meth.* **400** (1997) 181–183. doi:10.1016/S0168-9002(97)01031-0.

[24] G. D. Alkhazov, A. P. Komar, and A. A. Vorob’ev, *Ionization fluctuations and resolution of ionization chambers and semiconductor detectors*, *Nucl. Instrum. Meth.* **48** (1967) 1–12. doi:10.1016/0029-554X(67)90455-7.

[25] MKS Instruments, Andover, MA 01810, USA. www.mksinst.com.

[26] Bertan Model 375P High Voltage Power Supply. Fermilab Electronics Equipment Pool Catalog.

[27] Cremat, Inc., Watertown, MA 02472, USA. www.cremat.com.

[28] National Instruments Corp., Austin, TX 78759, USA. www.ni.com.

[29] SAES Pure Gas, Inc., San Luis Obispo, CA 93401, USA. www.saespuregas.com.

[30] R. W. Hendricks, *The gas amplification factor in xenon-filled proportional counters*, *Nucl. Instrum. Meth.* **102** (1972) 309–312. doi:10.1016/0029-554X(72)90728-8.

[31] G. F. Knoll, *Radiation Detection and Measurement.* John Wiley and Sons, Inc., New York, fourth ed., 2010.

[32] G. D. Alkhazov, *Statistics of electron avalanches and ultimate resolution of proportional chambers*, *Nucl. Instrum. Meth.* **89** (1970) 155–165. doi:10.1016/0029-554X(70)90818-9.

[33] H. Sipilä, *Energy resolution of the proportional counter*, *Nucl. Instrum. Meth.* **133** (1976) 251–252. doi:10.1016/0029-554X(76)90616-9.

[34] G. D. Alkhazov, *Mean value and variance of gas amplification in proportional counters*, *Nucl. Instrum. Meth.* **75** (1969) 161–162. doi:10.1016/0029-554X(69)90671-5.

[35] M. W. Charles and B. A. Cooke, *Proportional counter resolution*, *Nucl. Instrum. Meth.* **61** (1968) 31–36. doi:10.1016/0029-554x(68)90444-8.